*J. theor. Biol.* (1992) **155**, 295–333

# Pattern Formation in One- and Two-dimensional Shape-space Models of the Immune System

ROB J. DE BOER†§, LEE A. SEGEL‡ AND ALAN S. PERELSON†

†*Theoretical Division, Los Alamos National Laboratory, Mail Stop K710, Los Alamos, NM 87545, U.S.A. and*
‡*Department of Applied Mathematics and Computer Science, The Weizmann Institute of Science, Rehovot 76100, Israel*

(*Received on* 3 *January* 1991, *Accepted in revised form on* 10 *October* 1991)

A large-scale model of the immune network is analyzed, using the shape-space formalism. In this formalism, it is assumed that the immunoglobulin receptors on B cells can be characterized by their unique portions, or idiotypes, that have shapes that can be represented in a space of a small finite dimension. Two receptors are assumed to interact to the extent that the shapes of their idiotypes are complementary. This is modeled by assuming that shapes interact maximally whenever their coordinates in the space–space are equal and opposite, and that the strength of interaction falls off for less complementary shapes in a manner described by a Gaussian function of the Euclidean "distance" between the pair of interacting shapes.

The degree of stimulation of a cell when confronted with complementary idiotypes is modeled using a log bell-shaped interaction function. This leads to three possible equilibrium states for each clone: a virgin, an immune, and a suppressed state. The stability properties of the three possible homogeneous steady states of the network are examined. For the parameters chosen, the homogeneous virgin state is stable to both uniform and sinusoidal perturbations of small amplitude. A sufficiently large perturbation will, however, destabilize the virgin state and lead to an immune reaction. Thus, the virgin system is both stable and responsive to perturbations. The homogeneous immune state is unstable to both uniform and sinusoidal perturbations, whereas the homogeneous suppressed state is stable to uniform, but unstable to sinusoidal, perturbations. The non-uniform patterns that arise from perturbations of the homogeneous states are examined numerically. These patterns represent the actual immune repertoire of an animal, according to the present model.

The effect of varying the standard deviation $\sigma$ of the Gaussian is numerically analyzed in a one-dimensional model. If $\sigma$ is large compared to the size of the shape-space, the system attains a fixed non-uniform equilibrium. Conversely if $\sigma$ is small, the system attains one out of many possible non-uniform equilibria, with the final pattern depending on the initial conditions. This demonstrates the plasticity of the immune repertoire in this shape-space model. We describe how the repertoire organizes itself into large clusters of clones having similar behavior.

These results are extended by analyzing pattern formation in a two-dimensional (2-D) shape-space. A lattice mapping is employed, whose rules are rigorously derived from a simplified version of the underlying differential equations via a logarithmic

§ Present address: Bioinformatics Group, University of Utrecht, Padualaan 8, 3584 CH Utrecht, The Netherlands.

The work performed in this article was carried out under the auspices of the U.S. Department of Energy.



0022–5193/92/070295 + 40 $03.00/0 

transformation of variables. A novel feature of the lattice model is that the neighborhood of cell $(i, j)$ is centered around cell $(-i, -j)$. Thus, interactions are non-local. The 2-D patterns that emerge are reminiscent of those found in reaction–diffusion systems, and contain many hills and valleys. (In contrast with most reaction–diffusion models, pattern formation in this model is not dependent on long-range inhibition and short-range activation.) The scale of the pattern depends on neighborhood size, with small neighborhoods generating fine scale patterns with narrow peaks, and large neighborhoods generating large scale patterns with wide peaks and valleys. Both one- and two-dimensional models support patterns in which a fraction of the clones are not stimulated by network interactions. The fraction of such "disconnected clones" increases with both dimensionality and $\sigma$.

## 1. Introduction

Jerne (1974) postulated that the immune system functions as a network with a complexity comparable to that of the nervous system. The number of different lymphocyte clones, or idiotypes, involved in the immune network may be of order $10^6$ to $10^8$. Interactions amongst the clones depend on complementarities between the immunoglobulin receptors characteristic of each clone. The degree of binding of two idiotypes, usually measured by their equilibrium binding constant or affinity, depends on the generalized shapes of the two receptor molecules involved (Perelson & Oster, 1979). By generalized shape, we mean not only the average geometric shape of the binding region of the receptor molecule, but also factors such as the electric charge, dipole moments, and hydrophobicity. Recent structural determinations of antigen–antibody complexes (cf. Amit *et al.*, 1986; Stanfield *et al.*, 1990) highlight the importance of shape complementarity and show that in the binding region positive charges are complemented by negative ones (Sheriff *et al.*, 1987). Because cells in the immune system are constantly being generated in the bone marrow, stimulated to grow, and dying, one is led to conceive of the immune network as a vast collection of shifting clonal populations each characterized by a generalized shape $x$.

Attempts to model high-dimensional immune networks have utilized two different approaches to represent molecular shape and to compute complementarity between molecules. In one approach, the shape of receptors is associated with a binary string, and the degree of complementarity between bitstrings is employed to determine the degree of interaction between clones. The degree of interaction modifies the size of certain terms in a system of ordinary differential equations that determines the population size of each clone. In this approach the number of idiotypes incorporated in the network can vary, owing to the introduction of novel clones from a source meant to mimic the bone marrow, and owing to interactions among the clones present in the network (Farmer *et al.*, 1986; De Boer & Perelson, 1991). In a second approach put forward by Segel & Perelson (1988), and which we shall pursue here, shape is described by a vector of real numbers and a set of partial integro-differential equations in both shape and time variables determines the size of clonal populations. By finite difference methods, the partial differential equations can be converted into a set of ordinary differential equations. Thus, a discrete set of equations results but these are different from those in the bitstring model in that they have a different interaction kernel.

It is conceivable that an adequate characterization of essential shape variables can be accomplished by a relatively small number of measurements (Perelson & Oster, 1979). This would give a shape-space of some small finite dimension. Our earlier work (Segel & Perelson, 1988) was confined to a one-dimensional (1-D) shape-space; here we will extend this to a two-dimensional (2-D) shape-space. By contrast, in the bitstring approach the shape-space is the $l$-dimensional hypercube, where $l$ is the number of bits in the string used to represent shape. As we demonstrate below a major advantage of using a continuous shape-space is that standard analytical methods are available for partially analyzing system behavior.

The model that we analyze here is the one of a sequence of models that we have proposed, and studied extensively, in previous publications (De Boer, 1988; De Boer & Hogeweg, 1989*a–c*; De Boer *et al.*, 1990; De Boer & Perelson, 1991; Perelson & Weisbuch, 1992; Weisbuch *et al.*, 1990). For each B cell population, the model incorporates one differential equation with terms corresponding to a constant source of cells from the bone marrow, cell death, and proliferation in response to cell activation. The most crucial feature of the model is that the degree of activation is a log bell-shaped function of the total amount of stimulation a cell receives. Since a bell-shaped function has a region in which it increases and a region in which it decreases, the effect of increasing the stimulation can either be an increase or a decrease in proliferation. A steady state exists in each of the two regions. We have called these the *immune* state and the *suppressed* state, respectively. A third steady state exists when the degree of stimulation is negligible. This *virgin* state, is characterized by a balance between the source of cells from the bone marrow and the loss of cells due to cell death.

Here we study this model in a shape-space setting. Our aim is to come to a better understanding of repertoire development. The potential repertoire of our model immune system is the entire shape-space. Owing to network interactions, clones in some regions of the shape-space will be suppressed, some will be activated, and some will hardly be stimulated by other shapes in the immune network. Accordingly, we expect some spatial distribution of clone sizes throughout the network, where "spatial" refers to shape-space. This distribution, together with the spatial distribution of the degree of stimulation, defines our immune repertoire. We will show that the repertoire is very plastic in the sense that it can assume any of a large number of distinct spatial distributions. Further, we analyze the onset of pattern formation via linear stability theory. We find that the formation of patterns of the immune repertoire does not require a major feature postulated by Segel & Perelson (1988), inhibition and activation with different specificities.

We will first introduce the 1-D shape-space version of our model, and discuss its three uniform equilibrium states. We analyze the stability properties of these three states to both uniform and sinusoidal perturbations of small amplitude. We numerically study the model and then, based on our results, modify the model by introducing density-dependent growth to give more realistic non-uniform patterns. We then analyze a 2-D version of the model using a 2-D lattice mapping. (Readers unfamiliar with mathematical analysis may wish to skip the sections dealing with the stability of the uniform steady states.)

The most important immunological question that we address is whether or not the network, in its shape-space setting, will be able to combine a functional idiotypic network with a clonal organization of functionally disconnected antigen-reactive clones. In two recent reviews, Coutinho (1989) and Holmberg *et al.* (1989) argue that about 10–20% of clones form an idiotypic network. In their view, the other 80–90% of clones are disconnected from the network and form a clonal compartment of immunocompetent but resting lymphocytes that is responsible for immune responses to foreign antigens. The network is thought to select which T and B cell clones are expressed in an animal. This is what we call *repertoire selection.* In a shape-space model, the question of finding a combination of network and independent clonal organizations boils down to finding a mosaic of regions that are stimulated by the network and regions that are hardly stimulated. We will show this to be possible, but in our model the fraction of cells in each compartment does not agree with the Coutinho–Holmberg estimates.

Two other important immunological questions that we focus on is the ability of self-antigens to shape the repertoire of antibodies expressed within an animal, and the degree of *plasticity* of possible repertoires. First, if the antigenic experience of an animal is to be reflected in its immune repertoire, the immune system must be able to maintain a large variety of different patterns of antibody expression. We show that this is the case for our immune network model. Second, it appears that during B cell development exposure to self-antigens can cause the deletion or inactivation of self-reactive cells (cf. Goodnow *et al.*, 1990). In addition to the deletion of single clones, we show that network interactions can cause more global changes in the pattern of antibodies that an animal expresses. Thus, repertoires can be determined by interactions with both self- and foreign-antigens. This leads to the interesting speculation that each animal's immune system may be different. If this is the case, it may explain the observation that when immune responses are studied in inbred strains of mice, which are supposedly identical, one still observes considerable individual variability.

## 2. The One-dimensional Continuous Shape-space Model

### 2.1. FORMULATION

In principle our network model is composed of an infinite number of B cell and corresponding antibody populations of different shapes that may be ordered in a finite-dimensional shape-space. In order to facilitate analytic treatment we study a simple version of the model, in which we do not differentiate between B cells and free antibody, and in which we use a phenomenological log bell-shaped function to summarize the chemistry involved in receptor crosslinking and subsequent B cell activation. We have previously shown that more complex models that incorporate antibodies and crosslinking chemistry have similar steady states but in some parameter regimes tend to have oscillatory and/or chaotic behavior (De Boer *et al.*, 1990; Perelson & Weisbuch, 1991). Similar results have also been obtained by Stewart & Varela (1990) and Verela *et al.* (1988). Free antibody can be imagined as present, if

one assumes that there is always a constant number of free antibodies per lymphocyte. Note, however, that we have shown before that this can be an unrealistic assumption (De Boer & Perelson, 1991). An analysis with this assumption lifted has been published elsewhere (see Segel & Perelson, 1991).

We track the population levels $b(x, t)$ at time $t$ of B cells with receptors of shape $x$. We mainly consider here the simplest case wherein $x$ is a real number bounded by the half-length, $L$, of shape-space, i.e. $-L \leq x \leq L$. Later in the paper we examine the 2-D case where a second variable $y$ is introduced. Weisbuch (1990) and Weinand (1990, 1991) have explicitly dealt with 2-D and 3-D shape-spaces; Percus (1988) presents a model in which the dimension need not be specified. High-dimensional models restricted to a Bethe lattice have also been presented by Percus (1989) and Weisbuch *et al.* (1990). Recently, Stewart & Varela (1991) developed a 2-D shape-space model resembling the one presented here. Their model is further addressed in sections).

Writing $b(x, t)$ as $b$, we propose as the fundamental population balance equation of our model

$$\partial b/\partial T = M + b[Pf(h) - d].$$

Here $M$ is the constant source of cells from the bone marrow, $d$ is the per capita rate of cell death, $P$ is the maximum per capita rate of B cell proliferation, $f(h)$ defines the degree of activation, and $h$ is the total stimulation that the population receives from all other B cell populations in the shape-space. We will refer to $h$ as the *external field* or simply the *field* of the population. The model is non-dimensionalized by scaling the time $T$ to the rate at which B cells turn over:

$$\partial b/\partial t = m + b[pf(h) - 1], \tag{1}$$

where $t = Td$, $m = M/d$, and $p = P/d$.

The most crucial feature of this model is the shape of the activation function $f(h)$, which is taken to be the biphasic dose–response function

$$f(h) = \frac{h}{\theta_1 + h}\left(1 - \frac{h}{\theta_2 + h}\right) = \frac{h}{\theta_1 + h}\,\frac{\theta_2}{\theta_2 + h}, \tag{2}$$

where $\theta_2 \gg \theta_1$ (see Fig. 1). The first factor in $f$ increases from 0 to 1, reaching its half-maximal value at $\theta_1$, the second factor decreases from 1 to 0, reaching its half-maximal value at $\theta_2$. For $\theta_2 \gg \theta_1$, the maximum $\theta_2/(\sqrt{\theta_1} + \sqrt{\theta_2})^2$, is approximately 1. This maximum is attained at $h = \sqrt{\theta_1\theta_2}$. Because $0 \leq f(h) < 1$, we derive from eqn (1) that the B cells can maximally grow at a rate $p - 1$. Thus, in order to allow for net clonal expansion $p$ must be greater than 1. Since maximally stimulated cells divide about once every 16 hr, and cells live a few days (e.g. $d = 0{\cdot}5\ \text{day}^{-1}$), $p = 2$ is a typical non-dimensional rate of proliferation.

Below the maximum of $f(h)$, increasing $h$ increases $f(h)$; we call this the *stimulatory regime*. Above the maximum, increasing $h$ decreases $f(h)$; we call this the *suppressive regime*. Plotted as a function of $\log h$, the graph of $f(h)$ is a bell-shaped curve (Fig. 1). An important argument for the use of a log-shaped function is that receptor

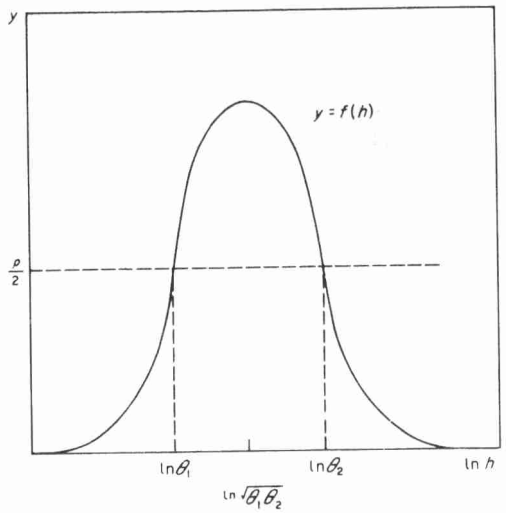


FIG. 1. Graph of the bell-shaped proliferation function, $f(h)$ given by eqn (2), vs. the logarithm of the field $h$. Equilibria involving proliferation, i.e. the immune and suppressed state, are close to the intersections of $f(h)$ with the line $y=p/2$, see the text.

crosslinking is involved in B cell activation. The fraction of cell surface receptors crosslinked by a ligand when plotted against the logarithm of the ligand concentration is called a crosslinking curve. For bivalent ligands the crosslinking curve is bell-shaped and symmetric around its maximum (Dembo & Goldstein, 1978; Perelson & DeLisi, 1980; Perelson, 1984).

The field $h(x; b)$ that is felt by B cells of shape $x$ in the presence of a population distribution $b=b(x, t)$ determines the degree of cell stimulation. To specify the field, we assume cells of shape $x$ are mainly stimulated by cells of complementary or near-complementary shape centered around $\hat{x}=-x$. For any shape $x$, let $g(x, \hat{x})b(\hat{x}, t)\,\mathrm{d}\hat{x}$ be the total stimulation (or field), $h$, that B cells of shape $x$ receive from B cells of shapes between $\hat{x}$ and $\hat{x}+\mathrm{d}\hat{x}$, where $\mathrm{d}\hat{x}$ is a small number. Then

$$h(x; b)=\int_{-L}^{L} g(x, \hat{x})b(\hat{x}, t)\,\mathrm{d}\hat{x}. \tag{3}$$

As in Segel & Perelson (1988), we assume that the affinity or degree of interaction between shapes $x$ and $\hat{x}$ decreases according to a Gaussian function $g(x, \hat{x})$ of the distance to the perfect match $x=-\hat{x}$:

$$g(x, \hat{x})=G(2\pi\sigma^2)^{-1/2}\exp\left[-(x+\hat{x})^2/2\sigma^2\right], \tag{4}$$

In (4) $G$ and $\sigma$ are constants determining the amplitude and width of the Gaussian, respectively. If each shape is complementary to only to a small fraction of all possible shapes, $\sigma \ll L$. Because we can scale $\theta_1$, and $\theta_2$, we can set $G=1$ without loss of

generality (De Boer & Perelson, 1991). This has the advantage that for $L \gg \sigma$

$$\int_{-L}^{L} g(x, \hat{x})\, d\hat{x} \approx 1. \tag{5}$$

For a multi-dimensional shape-space, we replace eqn (4) with

$$g(\boldsymbol{x}, \hat{\boldsymbol{x}}) = G(2\pi\sigma^2)^{-l/2} \exp\left[-(\boldsymbol{x}+\hat{\boldsymbol{x}})^2/2\sigma^2\right],$$

where $l$ is the dimension of the shape-space and $\boldsymbol{x}$ and $\hat{\boldsymbol{x}}$ are $l$-dimensional vectors. The use of different variances in different shape-space directions is also possible in this multi-dimensional model.

### 2.2. EQUILIBRIUM STATES

We have shown before (De Boer, 1988; Weisbuch *et al.*, 1990) that whenever $m \ll \theta_1 \ll \theta_2$ then eqn (1) has three spatially uniform equilibria $b(x, t) = \bar{b}$. We have called these the *virgin*, the *immune*, and the *suppressed* states, respectively. By eqns (3) and (5) the fields of the uniform states satisfy $h(x; \bar{b}) = \bar{b} = \text{constant}$, for all $x$. Each of the three states has its own typical range of values of the field. We greatly simplify our analysis by approximating $f(h)$ differently in each of the three states.

The virgin state corresponds to a situation in which B cells are hardly stimulated. This corresponds to the first region of the bell-shaped function where $h \ll \theta_1 \ll \theta_2$ and

$$f(h) \approx \frac{h}{\theta_1}. \tag{6a}$$

Recalling that for a uniform state, $h = \bar{b}$, the equilibrium value, $\bar{b}$, of the virgin state is then given by

$$\frac{\partial \bar{b}}{\partial t} = 0 = m + \frac{p}{\theta_1}\bar{b}^2 - \bar{b},$$

with solutions

$$\bar{b}^{\pm} = \frac{1 \pm \sqrt{1 - 4mp/\theta_1}}{2p/\theta_1}. \tag{6b}$$

A necessary condition for having a virgin state is that $\sqrt{1-4mp/\theta_1}$ is real, or

$$4mp < \theta_1. \tag{7}$$

Whenever eqn (7) holds, eqn (6b) yields two real positive solutions. The virgin state corresponds to the smaller of the two, i.e. to $\bar{b}^-$. (The solution $\bar{b}^+$ is close to $\theta_1$ and thus violates the condition $h \ll \theta_1$.) Choosing $m \ll \theta_1$, we approximate $\sqrt{1-4mp/\theta_1}$ by its first order Taylor expansion, and obtain

$$\bar{b} \approx m. \tag{8}$$

Since we choose $m \ll \theta_1$, eqn (6a) is a good approximation of eqn (2).

In the immune and the suppressed states B cells proliferate. Since a proliferating population based upon eqn (1) expands mainly by cell division, and not by receiving novel cells from the bone marrow, we neglect $m$ and observe that to a good approximation

$$\bar{b}[p(f(h))]=0, \qquad \text{or} \qquad f(h)=\frac{1}{p}, \qquad \text{for } \bar{b}>0. \tag{9}$$

For a clone in the immune state, further stimulation, i.e. a small increase of $h$, increases the rate of proliferation. This corresponds to the increasing region of $f(h)$ where $h<\sqrt{\theta_1\theta_2}$. If $\sqrt{\theta_1\theta_2}\ll\theta_2$, i.e. if $\sqrt{\theta_1}\ll\sqrt{\theta_2}$, then $\theta_2/(\theta_2+h)\approx 1$. Thus, we assume $\sqrt{\theta_1}\ll\sqrt{\theta_2}$, and in the region $m\ll h<\sqrt{\theta_1\theta_2}\ll\theta_2$, we approximate eqn (2) by

$$f(h)=\frac{h}{\theta_1+h}. \tag{10a}$$

Since $h=\bar{b}$, with (10a) eqn (9) becomes

$$f(h)=\frac{\bar{b}}{\theta_1+\bar{b}}=\frac{1}{p},$$

and hence

$$\bar{b}=\frac{\theta_1}{p-1}. \tag{10b}$$

Note that because $p>1$, $\bar{b}>0$.

When the system is in a suppressed state, further stimulation, i.e. an increase of $h$, decreases the rate of proliferation. This corresponds to the decreasing region of $f(h)$ where $h>\sqrt{\theta_1\theta_2}$. Therefore, by arguments similar to those given above, we approximate eqn (2) by

$$f(\bar{b})=\frac{\theta_2}{\theta_2+\bar{b}}. \tag{11a}$$

Since $h=\bar{b}$, eqn (9) becomes

$$f(h)=\frac{\theta_2}{\theta_2+\bar{b}}=\frac{1}{p},$$

and hence

$$\bar{b}=(p-1)\theta_2. \tag{11b}$$

Because $p-1\approx 1$, the B cell population levels in the uniform immune state, eqn (10b) and the uniform suppressed state, eqn (11b), are located around the respective half-saturation constants, $\theta_1$ and $\theta_2$, of the two saturation functions that make up $f(h)$.

### 2.3. STABILITY TO UNIFORM PERTURBATIONS

The linear stability analysis that we perform below follows that given in Segel & Perelson (1988) for a similar model having only one uniform equilibrium state. Treating each of our three equilibria separately, we analyze stability first to uniform and then to sinusoidal perturbations.

We first examine the effect of a small perturbation $b'(t)$ that is applied to each B cell population. For each of the equilibria

$$0 = m + \bar{b}[pf(\bar{b}) - 1]. \tag{12}$$

Writing

$$b(t) = \bar{b} + b'(t) \tag{13}$$

we find that

$$\frac{\partial(\bar{b} + b')}{\partial t} = \frac{\partial b'}{\partial t} = m(\bar{b} + b')[pf(\bar{b} + b') - 1]. \tag{14}$$

Upon substituting the first order Taylor expansion of $f(\bar{b} + b')$, employing eqn (12), and neglecting the second-order terms in $b'$ we obtain

$$\frac{\partial b'}{\partial t} = b'[pf(\bar{b}) + \bar{b}pf'(\bar{b}) - 1],$$

where $f'(\bar{b})$ denotes the derivative of $f(h)$ with respect to $h$ evaluated at $h = \bar{b}$. For stability we require $\partial b'/\partial t < 0$ when $b' > 0$, i.e.

$$pf(\bar{b}) + \bar{b}pf'(\bar{b}) - 1 < 0. \tag{15}$$

Employing our approximations (6a), (10a) and (11a) for the virgin, immune and suppressed states we obtain, respectively, the following versions of the stability condition (15):

$$2pm < \theta_1, \qquad \frac{p-1}{p} < 0, \qquad -\frac{p-1}{p} < 0. \tag{16a, b, c}$$

For the virgin state, stability condition (16a) is even less restrictive than condition eqn (7) for having a virgin state. Since $p \approx 2$, and $m \ll \theta_1$ both conditions will be satisfied. We conclude that the virgin state is stable to uniform perturbations. For the immune state, since $p > 1$ the stability condition (16b) is never satisfied, so that the immune state is unstable to uniform perturbations. For the suppressed state, since $p > 1$ the stability condition (16c) is always satisfied. The stability results for

TABLE 1

*Stability properties of the uniform steady states*

| State | Stability to perturbation | | Most dangerous perturbation |
|---|---|---|---|
| | Uniform | Sinusoidal | |
| Virgin | Stable | Stable | — |
| Immune | Unstable | Unstable | $\cos kx$ |
| Suppressed | Stable | Unstable | $\sin kx$ |

uniform perturbations are summarized in Table 1. The pattern of three alternating stable and unstable-steady states is of course standard for an equation of the form

$$\partial b/\partial t = \text{cubic in } b$$

that governs spatially uniform populations $b$. But it is advantageous to perform the simple calculation given above to obtain the growth and decay rates, for they form another point of comparison with the numerical analysis.

### 2.4. STABILITY TO SINUSOIDAL PERTURBATIONS

Consider a perturbation that is exponential in time and sinusoidal in space. For the time being consider a shape-space of infinite domain. We search for perturbations that can destabilize the uniform steady states. As is conventional, we examine

$$b'(x, t) = \beta\, e^{\lambda t + ikx} + \beta^* e^{\lambda^* t - ikx}, \tag{17}$$

where the asterisk denotes the complex conjugate, and the real number $k$ is the wavenumber of the perturbation. In higher dimensions, we use a similar perturbation but replace $kx$ by $\boldsymbol{k} \cdot \boldsymbol{x}$, where $\boldsymbol{k}$ and $\boldsymbol{x}$ are vectors. We assume $k \neq 0$, so that the perturbation is sinusoidal and leaves the average value of $b$ unchanged. Equation (17) is a corrected version of the corresponding eqn (A.11) in Segel & Perelson (1988). Jaeger (Weizmann Institute) pointed out the error to us, and put forward a corrected proof that $\lambda$ is real, which is incorporated into the stability analysis given below.

Employing eqns (3) and (17), and redefining the Gaussian function as $g(x+\hat{x})$, we find that the perturbation of the field $h$ due to $b'$ is

$$h(b') = \int_{-\infty}^{\infty} g(x+\hat{x})[\beta\, e^{\lambda t + ik\hat{x}} + \beta^* e^{\lambda^* t - ik\hat{x}}]\, d\hat{x}.$$

With the substitution $z = x + \hat{x}$ we obtain

$$\begin{aligned} h(b') &= \int_{-\infty}^{\infty} g(z)[\beta\, e^{\lambda t + ik(z-x)} + \beta^* e^{\lambda^* t - ik(z-x)}]\, dz \\ &= \hat{g}(k)[\beta\, e^{\lambda t - ikx} + \beta^* e^{\lambda^* t + ikx}]. \end{aligned} \tag{18a}$$

Here $\hat{g}$ is the Fourier transform

$$\hat{g}(k)=\int_{-\infty}^{\infty} e^{ikz}g(z)\,dz=e^{-k^2\sigma^2/2}. \tag{18b}$$

In analogy to eqns (12–14) we write

$$\frac{\partial(\bar{b}+b')}{\partial t}=\frac{\partial b'}{\partial t}=m+(\bar{b}+b')\left[pf\left(\int g(x+\hat{x})(\bar{b}+b'(\hat{x}))\,d\hat{x}\right)-1\right].$$

Employing eqn (5) we reshuffle this into

$$\frac{\partial b'}{\partial t}=m+(\bar{b}+b')\left[pf\left(\bar{b}+\int g(x+\hat{x})b'(\hat{x})\,d\hat{x}\right)-1\right],$$

which, upon expanding $f(.)$ around $\bar{b}$ yields

$$\frac{\partial b'}{\partial t}=m+(\bar{b}+b')\left[pf(\bar{b})+pf'(\bar{b})\int g(x+\hat{x})b'(\hat{x})\,d\hat{x}-1\right].$$

Upon neglecting the second-order term of $b'$, and using eqn (12), this can be rewritten as

$$\frac{\partial b'}{\partial t}=b'[pf(\bar{b})-1]+\bar{b}pf'(\bar{b})\int g(x+\hat{x})b'(\hat{x})\,d\hat{x}.$$

Employing eqns (17) and (18a), we find that

$$\begin{aligned}\lambda\beta\, e^{\lambda t+ikx}+\lambda^*\beta^*\, e^{\lambda^* t-ikx}=&[\beta\, e^{\lambda t+ikx}+\beta^*\, e^{\lambda^* t-ikx}](pf(\bar{b})-1)\\&+[\beta\, e^{\lambda t-ikx}+\beta^*\, e^{\lambda^* t+ikx}]\bar{b}pf'(\bar{b})\hat{g}(k).\end{aligned} \tag{19}$$

We write $\lambda=\lambda_r+i\lambda_i$; $\beta=\beta_r+i\beta_i$. If $\lambda_i\neq 0$, in (19) the coefficients of $e^{i\lambda_i t}$ and $e^{-i\lambda_i t}$ must both vanish. This gives

$$[\lambda-(pf(\bar{b})-1)]\beta\, e^{ikx}-\bar{b}pf'(\bar{b})\hat{g}(k)\beta\, e^{-ikx}\equiv 0,$$

together with its complex conjugate. It follows that (for $\beta\neq 0$), $\lambda=pf(\bar{b})-1$, which contradicts $\lambda_i\neq 0$. Hence, $\lambda$ must be real. One can therefore cancel $e^{\lambda t}$ and $e^{\lambda^* t}$ in eqn (19), wherein for $k\neq 0$, the coefficient of $\exp(ikx)$ must vanish separately from the coefficient of $\exp(-ikx)$. Thus,

$$\beta[pf(\bar{b})-1-\lambda]+\beta^*\bar{b}pf'(\bar{b})\hat{g}(k)=0, \tag{20}$$

together with its complex conjugate. Taking the real and imaginary parts of eqn (20) we obtain

$$\beta_r[pf(\bar{b})-1-\lambda+\bar{b}pf'(\bar{b})\hat{g}(k)]=0,\qquad \beta_i[pf(\bar{b})-1-\lambda-\bar{b}pf'(\bar{b})\hat{g}(k)]=0.$$

Non-trivial solutions result when

$$\beta_r = 0,\ \beta_i \neq 0,\ \lambda = \lambda^- \qquad \text{and} \qquad \beta_r \neq 0,\ \beta_i = 0,\ \lambda = \lambda^+, \tag{21}$$

where

$$\lambda^{\pm} = pf(\bar{b}) - 1 \pm \bar{b}pf'(b)\, e^{-k^2\sigma^2/2}, \qquad k \neq 0, \tag{22}$$

and eqn (19) has been used to substitute for $\hat{g}(k)$. We now use this result, i.e. the values of $\lambda^+$ and $\lambda^-$, to examine the stability of the virgin, immune, and suppressed steady states to sinusoidal perturbations.

In the virgin state, $\bar{b} \approx m$, we approximate eqn (2) by eqn (6a), obtaining

$$f(\bar{b}) = \frac{\bar{b}}{\theta_1}, \qquad f'(\bar{b}) = \frac{1}{\theta_1}.$$

Substitutiing this into eqn (22) yields

$$\lambda^{\pm} = \frac{pm}{\theta_1} - 1 \pm \frac{pm}{\theta_1} e^{-k^2\sigma^2/2}. \tag{23}$$

For $m \ll \theta_1$, the term before the $\pm$ symbol is negative. Instability, i.e. $\lambda > 0$, can therefore only be obtained for $\lambda^+$. The largest contribution of the term following the $\pm$ symbol in eqn (23) is obtained when $e^{-k^2\sigma^2/2}$ reaches its maximal value, which equals unity for $k = 0$. Hence, we obtain as a sufficient condition for stability

$$\lambda^+ = \frac{2pm}{\theta_1} - 1 < 0. \tag{24a}$$

This condition is equal to the requirement for stability of the virgin state to a uniform perturbation [i.e. eqn (16a)] and is satisfied as long as the virgin state exists. We conclude that the virgin state is stable to both uniform and sinusoidal perturbations (see Table 1).

In the immune state, $\bar{b} = \theta_1/(p-1)$, we neglect $m$ and approximate eqn (2) by eqn (10a), i.e.

$$f(\bar{b}) = \frac{\bar{b}}{\theta_1 + \bar{b}} = \frac{1}{p} \qquad \text{and} \qquad f'(\bar{b}) = \frac{\theta_1}{(\theta_1 + \bar{b})^2} = \frac{(p-1)^2}{\theta_1 p^2}.$$

Hence, eqn (22) simplifies into

$$\lambda^{\pm} = \pm \frac{p-1}{p} e^{-k^2\sigma^2/2}. \tag{24b}$$

Because $p > 1$, $\lambda^+ > 0$ and the immune state is unstable to sinusoidal perturbations. Substituting $\lambda = \lambda^+$, $\beta_r \neq 0$ and $\beta_i = 0$, into eqn (17) yields

$$b'(x, t) = e^{\lambda^+ t}\beta_r[e^{ikx} + e^{-ikx}] = 2\beta_r e^{\lambda^+ t} \cos kx,$$

and hence destabilizing perturbations are of the form $\cos kx$ (see Table 1).

In the suppressed state, $\bar{b}(p-1)\theta_2$, we neglect $m$ and approximate eqn (2) by eqn (11a), i.e.

$$f(\bar{b})=\frac{\theta_2}{\theta_2+\bar{b}}=\frac{1}{p} \qquad \text{and} \qquad f'(\bar{b})=-\frac{\theta_2}{(\theta_2+\bar{b})^2}=-\frac{1}{p^2\theta_2}.$$

Hence eqn (22) simplifies into

$$\lambda^{\pm}=\mp\frac{p-1}{p}\,e^{-k^2\sigma^2/2}. \tag{24c}$$

Since $p>1$, $\lambda^{-}>0$ and the suppressed state is unstable to sinusoidal perturbations. Substitution of $\beta_r=0$ and $\beta_i\neq 0$, into eqn (17) yields

$$b'(x,t)=e^{-\lambda t}\beta_i i[e^{ikx}-e^{-ikx}]=-2\beta_i\,e^{-\lambda t}\sin kx,$$

and hence destablishing perturbations are of the form $\sin kx$ (see Table 1).

Small sinusoidal perturbations of the immune state and suppressed state will both grow most rapidly when $\exp(-k^2\sigma^2/2)$ is maximal, i.e. for an infinite wavelength $k=0$. However, the states differ with respect to the form of the "most dangerous" sinusoidal perturbation, i.e. whether it is $\sin kx$ or $\cos kx$. It is important to realize that, with respect to $x=0$, perturbations of the form $\sin x$ are asymmetric in the shape-space, whereas those of the form $\cos x$ are symmetric. Thus, if a perturbation of the form $\sin x$ increases certain populations around shape $x$, the complementary shapes around $-x$ decrease. Because these complementary shapes comprise the field $h(x)$, perturbations of the form $\sin kx$ induce an opposite change in each population and its field. Conversely, since perturbations of the form $\cos kx$ are symmetric around $x=0$, cosinusoidal perturbations causes both populations and fields to change in the same direction.

For the immune state, in which $\cos kx$ is most dangerous, this means that any increased population gains an increased field. Since the population is in the stimulatory regime, this causes the increased populations to increase further. Similarly, any decreased population will decrease. Additionally, as $k\to 0$, a $\cos kx$ perturbation tends to increase all shapes uniformly. Indeed, as $k\to 0$ the requirement for stability to cosinusoidal perturbations [see eqn (24b)] becomes identical to that for stability to uniform perturbations, eqn (16b).

For the suppressed state, in which the asymmetric perturbation $\sin kx$ is destabilizing, this means that any increased population gains a decreased field. Since the population is in the suppressive regime, this causes the increased populations to increase further. Similarly, any decreased population will decrease. Additionally, as $k\to 0$, $\sin kx$ perturbs all shapes of equal sign in the same direction. Thus, one side of the shape-space populations increases, while on the other side populations decrease. Since the changes on the positive side of the shape-space will reinforce the rate of change on the negative side of shape-space, and vice versa, such a perturbation grows rapidly.

It is easy to extend our stability results to the case where shape-space is confined to the interval $-L\leq x\leq L$, with periodic boundary conditions. In considering the

infinite domain, for example, destabilizing perturbations to the immune state take the form of $\cos kx$ for any positive $k$. Now $k$ is restricted to the values $n\pi/L$, where $n$ is a positive integer.

## 3. A Discrete One-dimensional Shape-space

### 3.1. FORMULATION

So far in our analysis we have treated shape-space as if it were continuous. In order to numerically solve eqns (1–5) that determine our model we need to discretize the problem. Although this can be done with any of a number of well-studied procedures, we prefer to describe a discrete formulation of our model that can stand on its own as an immune network model. This is the same philosophy that underlies the numerical work in Segel & Perelson (1988).

In the discrete formulation of the one-dimensional problem, the shape-space is divided into subintervals of width $\Delta$. Let $b_i(t)\Delta$ represent the population size of a set of clones of related shape centered around $b(x, t)$, where $x = i\Delta$, $i = -N, \ldots, N$. Let the interval of shapes represented by $b_i$ be symmetrically distributed around $b(x, t)$, i.e. have width $\Delta/2$ on each side of $b(x, t)$. Thus, the entire shape-space is now defined on $-L - \Delta/2 \leq x \leq L + \Delta/2$. Since there are $2N+1$ intervals, each of width $\Delta$, $L = N\Delta$. If periodic boundary conditions are used, then the extension of shape-space beyond $L$ is not needed. In this case, we set $b_{-N} = b_N$ and hence we map the region of width $\Delta/2$ to the left of $-L$ into the region of width $\Delta/2$ to the left of $L$, and similarly for the regions to the right of $L$ and $-L$. Despite the apparent complexity, we choose this symmetric representation so that $b_0$ represents clones distributed around the origin of shape-space.

In the discrete representation,

$$b_i(t) = b(x_i, t)\Delta, \qquad i = -N, \ldots, N,$$

where $b(x, t)$ is a density having units of number/unit length of shape, whereas $b_i$ has units of number. In this formulation we can either view the $b_i$ as representing "superclones", i.e. a set of clones of sufficiently similar shape that their behavior can not be distinguished, or, if we have a fine enough grid, as the set of all possible clones in the animal.

We now construct a set of discrete equations that are the counterparts of eqns (1–5). Thus,

$$\mathrm{d}b_i/\mathrm{d}t = m_i + b_i[pf(h_i) - 1], \tag{25a}$$

where $m_i$ is the rate of supply of clones of type $i$. The activation function $f(\cdot)$ is still given by eqn (2). The counterpart of eqn (3) specifying the field is

$$h_i = \sum_{j=-N}^{N} g(i, j)b_j(t)\Delta. \tag{25b}$$

Because we have discretized shape-space, the Gaussian now becomes

$$g(i,j) = G(2\pi\sigma^2)^{-1/2} \exp\left[-(i+j)^2\Delta^2/2\sigma^2\right]. \tag{25c}$$

We employ periodic boundary conditions, so that $b_{-N} = b_N$, and our system consists of a set of $2N$ ordinary differential equations. If the tails of the Gaussian reach the boundaries we wrap them around the domain, allowing the distance in the Gaussian to increase. Thus, the field becomes

$$h_i = \sum_{j=-\infty}^{\infty} g(i,j) b_j(t) \Delta, \tag{25d}$$

where $b_j$ is assumed to be $2N$ periodic, i.e. $b_j = b_{j+2N} = b_{j-2N}$.

In the discrete approach one can view the system (25a) of differential equations as forming the true model, which describes the interactions among a set of $2N$ clones. The continuous system of partial differential equations then is an approximate description and presumably a good one when $N$ is large. An alternative approach is to view the partial differential equations as the true model. Then any of a number of discretizations are possible, some more accurate then the simple trapezoidal rule approximation for the integral in eqn (25b).

### 3.2. SIMULATION OF THE DISCRETE MODEL

We simulated the discrete model by numerical integration. Since the space is sampled according to the Gaussian function $g(.)$, and because $\Delta$ defines the step size in space, we define $n \equiv \sigma/\Delta$, so that $n$ is the number of intervals used to approximate one standard deviation of the Gaussian. [The paper of Weisbuch (1990) can be regarded as a study of situations in which $\sigma < \Delta$.] We typically choose $n = 5$, and test the accuracy of the approximation by increasing $n$, which should not affect the results. With no loss of generality the size, $L = N\Delta$, of the shape-space is chosen as $L = 1$. (This can be accomplished by introducing a dimensionless shape variable $x/L$.) The number of differential equations needed, $2N$, is then determined by $N = L/\Delta = nL/\sigma$. Increasing the accuracy of the spatial approximation, i.e. increasing $n$, thus increases the number of differential equations.

In order to compare our analytic derivations with our numerical analysis, and hence to check both, we simulated this discrete system with periodic boundary conditions. In the numerical approximation the maximum wavelength is $2L$. Owing to the periodic boundary conditions the wave has to repeat itself beyond $L$ and $-L$. First, for the virgin state, $\bar{b} = m$, we confirmed the stability to both uniform and sinusoidal perturbations (not shown). Second, for the immune state, we showed that a uniform perturbation that increases the population size of clones that were initially at the immune state, $\bar{b} = \theta_1$, causes all of the clones to increase in size until the suppressed state, $\bar{b} = \theta_2$, is attained. Conversely, a uniform negative perturbation, that decreases the population size of all clones at the immune state, causes clones to decrease uniformly in size until the virgin state, $\bar{b} = m$, is attained (not shown).

Recall that the immune state is unstable to perturbations of the form $\cos kx$, whereas the suppressed state is unstable to perturbations of the form $\sin kx$. Figure 2(a) shows that a perturbation of the immune state of the form $\sin \pi x$ has a tendency to damp out. However, due to non-linear effects the network fails to return to the immune state, but attains the uniform virgin state. Figure 2(b) shows a perturbation of the immune state of the form $\cos \pi x$. The perturbation increases in amplitude, spreads, and approaches the uniform suppressed state $\bar{b} = \theta_2$, from where it grows

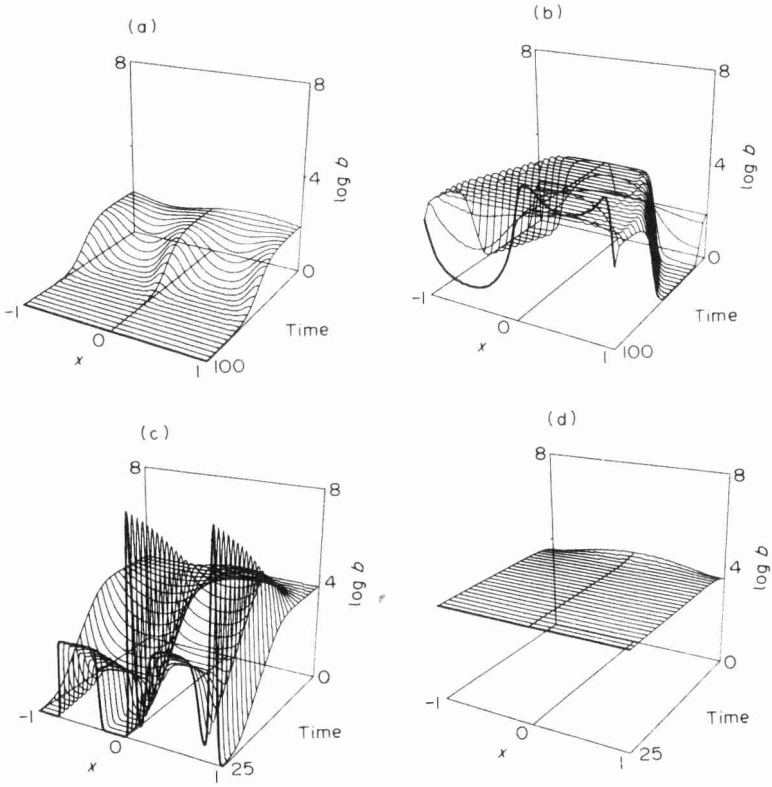


FIG. 2. Development of sinusoidal perturbations to the uniform immune and the uniform suppressed state. Solution of the system (25) with periodic boundary conditions, $-L \leq x \leq L$. Parameters: $m_i = 1$, $p = 2$, $\theta_1 = 10^2$, $\theta_2 = 10^4$, $L = 1$, $\sigma = 0{\cdot}045$, $n = 5$, $\Delta = 0{\cdot}009$, $N = 112$. The final distribution is shown as a heavy line. (a) A perturbation around the immune state, $\bar{b} = 100$, of the form $50 \sin x\pi/L$, damps out during the first few time steps. Because the increased populations decrease more rapidly than the decreased populations increase, the increased populations receive insufficient stimulation at the time they attain the immune state. Hence, they decrease further, and the system finally attains the virgin state $\bar{b} = m$. (b) A perturbation around the immune state, $\bar{b} = 100$, of the form $10 \cos x\pi/L$, increases and spreads through the shape-space. In the middle region the uniform suppressed state is attained. The network leaves the suppressed state via a distribution of the form $\sin x$. (c) A perturbation around the suppressed state $\bar{b} = 10^4$ of the form $10 \sin x\pi/L$, grows rapidly. The network finally approaches a pattern with narrow but high peaks. (d) A perturbation around the suppressed state $\bar{b} = 10^4$ of the form $10 \cos x\pi/L$ damps out and returns to the uniform suppressed state.

further in the form of sin $\pi x$. As predicted, the suppressed state was found stable to uniform perturbations. Figure 2(c) shows the effects of a perturbation of the form sin $\pi x$ to the suppressed state $\bar{b} = \theta_2$. The perturbation grows monotonically until non-linear effects come into play. Conversely, a perturbation of the form cos $\pi x$ decreases in amplitude [Fig. 2(d)]. These observations confirm our analytic results.

The simulations displayed in Fig. 2(b) and (c) did not attain an equilibrium distribution. The simulations were terminated since some of the populations grow very large by self-stimulation. This is illustrated in Fig. 3(a), which displays the distribution of clones and fields at $t = 50$. These results are attained by continuation

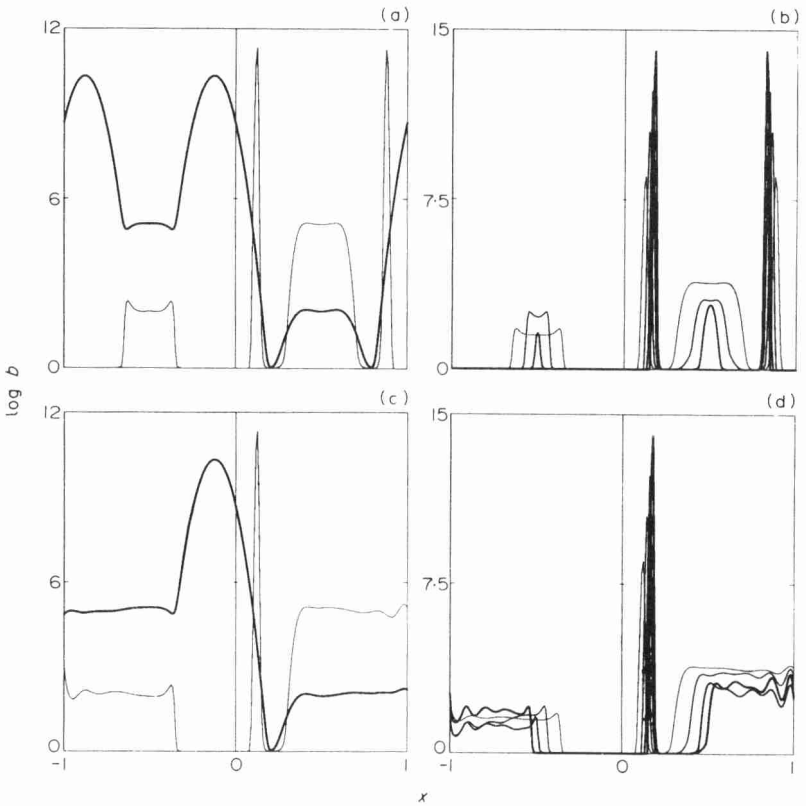


FIG. 3. The distribution of the B cell populations (light lines) and of the fields (heavy lines) that are attained long after a destabilizing perturbation ($b' = 10 \sin x\pi/L$) of the suppressed state. Periodic boundary conditions with parameters as in Fig. 2. (a) The distribution at $t = 50$ on a logarithmic scale ranging to $10^{12}$ cells. The two, unrealistically large, peaks are sustained through self-stimulation. The corresponding peaks in the fields reach the opposite part of the shape-space by crossing at $x = 0$ and $x = L$. The low affinity that is typical of the tail of the Gaussian distribution is counterbalanced by a very large population size. (b) The time evolution of these spiky patterns on a logarithmic scale ranging to $10^{15}$ cells. The B cell distributions are displayed at $t = 50$, 100, 150, 200. (c) As in (a) but for fixed boundary conditions. Now the shape-space is dominated by a single large peak, which is a low affinity autobody. (d) As in (b) but for fixed boundary conditions.

of the simulation shown in Fig. 2(c). Figure 3(a) displays two peaks of about $10^{11}$ cells, having a stimulatory field value. Closer inspection shows that the field of each peak is comprised of a contribution from the tail of the Gaussian centered around the shape complementary to that peak. In other words, the clones stimulate themselves. To see how this works, consider the effect of a single clone at $x = x_1$, where $x_1 > 0$. Thus, let

$$b(x) = b_1 \delta(x - x_1),$$

where $\delta$ denotes the delta function. Then, by eqn (3),

$$h(y) = \int g(x+y) b(x)\, dx = b_1 g(x_1 + y). \tag{25e}$$

The field is maximal at $y = -x_1$ and falls towards zero as $y$ approaches $x_1$. If, at some value $\hat{y}$, $h(\hat{y}) \approx \sqrt{\theta_1 \theta_2}$ then a clone at $\hat{y}$ will be maximally stimulated. If this maximal stimulation occurs at $\hat{y} = x_1$, then the clone at $x_1$ will stimulate itself maximally. This will occur if $b_1 g(2x_1) \approx \sqrt{\theta_1 \theta_2}$ or $x_1 = \sigma\sqrt{2 \log \eta}/2$, where $\eta = b_1 / \sqrt{2\pi\sigma^2 \theta_1 \theta_2}$. Thus, $x_1$ is of order $\sigma$, i.e. near the origin. Notice that the larger $b_1$ is, the further from the origin is the clone that maximally stimulates itself. Thus we expect the peak near the origin to move gradually to the right as it grows, which in fact is observed in the simulations.

Self-stimulation of clones near the origin makes sense because shapes near zero are supposed to match themselves closely. B cells clones that stimulate themselves strongly have been discovered in mice and are called *autobodies* (Kang & Köhler, 1986*a*, *b*). In our model a low affinity autobody can grow large enough to sustain its own proliferation, and—as a side effect—dominate a large proportion of the shape-space. The other peak in Fig. 3(a) stimulates itself due to the periodic boundary condition. In Fig. 3(b) we continue the stimulation further, showing the B cell distribution at $t = 50$, 100, 150, 200. This shows that the peaks keep on increasing, moving further outwards into the tail of the Gaussian distribution. The population levels are unrealistically high, and we end up (at $t = 200$), with a repertoire containing only two species. In Fig. 3(c)–(d) we repeat the simulations for a system wherein $b(x, t) \equiv 0$ when $x$ is outside the interval $[-L, L]$. Under these conditions there is no contribution to the field from clones outside the interval. We term this system as one with *fixed boundaries*. We now only find the autobody peak, but its unrealistic increase to extremely large populations is the same.

In reality shape-spaces are neither infinite nor periodic. Having confirmed our analytic derivations, which were done for an infinite domain, it seems more realistic to abandon the periodic boundary conditions and assume fixed boundaries for our further exploratory numerical work. Fixed boundaries only affect the field of the clones close to the boundaries. For instance, in a uniform state, $b = \bar{b}$, the field of the clone in the middle still approximates $h = \bar{b}$, but shapes at the boundary have a field that is closer to $h = \bar{b}/2$ than to $h = \bar{b}$. This non-uniform distribution of the field alters the uniform suppressed state $\bar{b} = (p-1)\theta_2$, but the alteration is confined to the vicinity of the boundaries. Because the suppressed state is unstable to sinusoidal

perturbations, and because completely uniform perturbations are unrealistic anyway, this hardly changes the interpretation of our results.

### 3.3. THE PROBLEM OF LARGE POPULATION SIZES

Assuming fixed boundaries eliminates the possibility of self-stimulation via the edges of the shape-space, but fails to solve the problem raised by the autobodies centered around $x=0$. The reason why a small degree of self-stimulation causes populations to be so large can be understood by writing the ordinary differential equation

$$\mathrm{d}b/\mathrm{d}t = m + b[pf(\varepsilon b) - 1], \tag{26a}$$

where $b(t)$ is the population at time $t$ of an autobody of shape $x_1$, $h=\varepsilon b$ defines the degree of self stimulation, and, from the material under eqn (25e), $\varepsilon = g(2x_1)$. In analogy with the derivation of the three uniform equilibrium states, i.e. eqns (8), (10b), and (11b), we now obtain

$$\bar{b}=m, \qquad \bar{b}=\frac{\theta_1}{\varepsilon(p-1)}, \qquad \bar{b}=\frac{(p-1)\theta_2}{\varepsilon}, \tag{26b}$$

for the virgin, the immune, and the suppressed state of the autobody, respectively. As in the stability analysis for uniform perturbations, one can show that the virgin and the suppressed state are stable, and that the immune state is unstable. Thus, we expect that an autobody, once stimulated, will grow sufficiently large so that it ultimately suppresses itself. The counterintuitive property of the self stimulation is that a decrease of the degree or self stimulation, $\varepsilon$, increases the equilibrium population in both the immune and the suppressed states. Instead of interactions fading away at the tails of the Gaussian distributions they may become more pronounced! We consider this point further in section 5.

A simple solution to the problem of large population sizes is to incorporate a self-limiting term in the growth equation for each population. Thus, we multiply the maximum proliferation rate $p$ by the density dependent function $r(b)$, so that eqn (1) is replaced by

$$\partial b/\partial t = m + b[pf(h)r(b) - 1], \tag{26c}$$

where $r(b)$ is

$$r(b)=\frac{\theta_3}{\theta_3+b}.$$

Instead of $r(b)$ a variety of other functions could be used. For example, Segel & Perelson (1988) suggested $\mathrm{e}^{-\lambda b}$. The logistic type term, $(1-b/b_{\max})$, could also be used. We prefer $r(b)$ for two reasons. First, unlike the logistic term there is no strict maximum population size. Populations can get to be larger than $\theta_3$ but not much larger. Thus, the limit to population growth is somewhat elastic. This is more akin to what happens in the immune system, where the total number of lymphocytes is

controlled but can still rise during infections. Additionally, because a logistic term allows for negative growth rates, it requires the assumption that above the maximum population size stimulated clones decay more rapidly than non-stimulated clones. This need not be the case in the immune system. As to the exponential term, it also gives rise to an elastic limit, but it has the disadvantage that to find the steady-state population size one needs to solve a transcendental equation rather than a polynomial.

Incorporating the density-dependent function $r(b)$ into the model will have no effect on the stability results as long as $r(b)$ only plays a role at population densities that are much larger than the three equilibrium population levels $\bar{b}=m$, $\bar{b}=\theta_1/(p-1)$, and $\bar{b}=(p-1)\theta_2$. The equilibrium value that is attained by a population, $b$, limited by the growth limitation only, i.e. for $f(h)\approx 1$, is

$$\frac{\theta_3}{\theta_3+b}=\frac{1}{p}, \qquad \text{hence} \qquad \bar{b}=(p-1)\theta_3, \tag{26d}$$

which is of order $\theta_3$. Setting $\theta_3 \gg \theta_2 \gg \theta_1 \gg m$, ensures that $r(b)\approx 1$ in the virgin, immune and suppressed equilibrium states. Whenever $r(b)\approx 1$ it can be omitted from eqn (26c), reducing it to eqn (1), that we have used for the stability analysis.

One can also show formally that adding $r(b)$ to the model does not add new uniform equilibrium states. Consider a region where $r(b)$ plays a functional role, i.e. let $\bar{b}$ a uniform B cell population of order $\theta_3$. Because $h=\bar{b}=\theta_3 \gg \theta_2 \gg \theta_1$,

$$\frac{h}{\theta_1+h}\approx 1, \qquad \text{and} \qquad \frac{\theta_2}{\theta_2+h}\approx 0.$$

As a result, $f(h)\approx 0$. However, if $f(h)\approx 0$, eqn (26a) reduces to

$$\frac{\partial b}{\partial t}\approx m-b,$$

which has the virgin state, $\bar{b}=m$, as the only equilibrium solution. Since $m \ll \theta_1 \ll \theta_2 \ll \theta_3$, $\bar{b}$ is not of order $\theta_3$, which contradicts our assumption. Hence, besides the virgin, immune and suppressed states, there is no additional uniform equilibrium in the region where $\bar{b} \gg \theta_2$.

### 3.4. PLASTICITY

In Fig. 4 we show the time evolution of a network incorporating the self-limitation $r(b)$ with $\theta_3=10^6$. The variance is equal to that studied in Figs 2 and 3, i.e. $\sigma=0{\cdot}045$. As a non-uniform initial condition, we now assign to each population a value that is randomly distributed around the suppressed state with 10% standard deviation. The main difference with the results shown in Figs 2 and 3 is that an equilibrium distribution is now attained. In the equilibrium some populations are close to the maximum $\theta_3$, while other populations attain values around the immune and suppressed states. As was to be expected, the autobody close to the origin $x=0$ grows to the maximum level. One can calculate the affinity at which the autobody

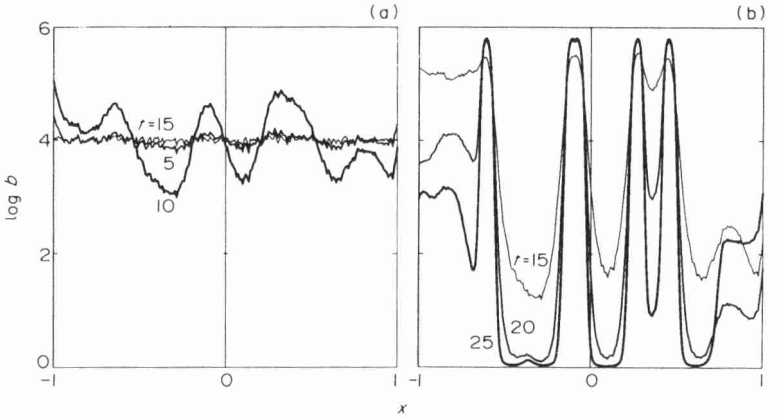


FIG. 4. Time evolution of a network governed by eqn (26c) with fixed boundaries. Parameters as in Fig. 2 except $\theta_3 = 10^6$. In the initial state populations are randomly distributed around $\theta_2$ with 10% standard deviation. The B cell distributions attained at $t = 0$, 5, 10 are shown in (a), those attained at $t =$ 15, 20, 25 are shown in (b).

will be located. From eqn (26a), in order to stimulate itself $\theta_1 < \varepsilon\bar{b} < \theta_2$. From (26c), $\bar{b}(p-1)\theta_3$. Since maximal growth is attained at $\varepsilon\bar{b} = \sqrt{\theta_1\theta_2}$, the autobody population is expected to be centered around

$$\varepsilon = \frac{\sqrt{\theta_1\theta_2}}{(p-1)\theta_3},$$

which for our parameters is $\varepsilon = 10^3/10^6 = 10^{-3}$. Further, since $\varepsilon = g(2x_1)$, we find for the parameters in Fig. 4, $x_1 = 0{\cdot}095$.

In Fig. 5 we display a number of different equilibrium distributions as a function of the standard deviation $\sigma$. (Note that $\Delta$ and $N$ vary with $\sigma$, but that this should not affect the results.) The main result is that the smaller the variance the more peaks there are in the repertoire. Interestingly, we find an organization that goes beyond the level of individual peaks. We find clusters of clones that are all distributed around either the immune or the suppressed state. The size of the clusters is much larger than the width of the Gaussian. The entire cluster interacts with another cluster at the opposite part of the shape-space. We may thus speak of a cluster of idiotypes and a cluster of anti-idiotypes. If the idiotypic cluster is in the immune state, the anti-idiotype cluster is in the suppressed state (and vice versa). Within each cluster we find an array of peaks and valleys of clone sizes distributed around the average state. Clones in interacting clusters behave in a co-ordinated way. While the network is slowly attaining an equilibrium distribution, idiotypic and anti-idiotypic clusters oscillate as if they were two interacting antibody species (not shown).

We have noted earlier in the bitstring models that clones may organize into larger units that have similar properties in the network (De Boer & Perelson, 1991). The present results suggests that these clusters may be of any size [see e.g. Figs 5(a) and

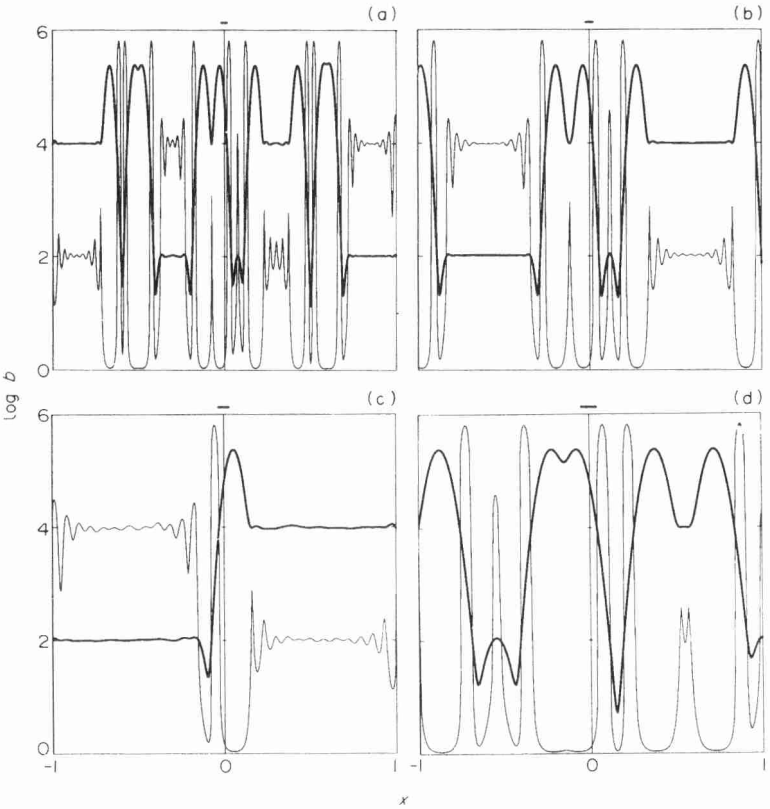


FIG. 5. The distributions of B cell population sizes (light lines) and fields (heavy lines) for the network of Fig. 4, showing how the results depend on the range of interaction in shape-space, i.e. on $\sigma$. Parameters as in Fig. 2 except $\theta_3 = 10^6$. Displayed is the equilibrium repertoire attained at $t = 1000$. (a) $\sigma = 0{\cdot}016$, $\Delta = 0{\cdot}003$, $N = 316$. (b) $\sigma = 0{\cdot}022$, $\Delta = 0{\cdot}004$, $N = 224$. (c) $\sigma = 0{\cdot}032$, $\Delta = 0{\cdot}006$, $N = 158$. (d) $\sigma = 0{\cdot}045$, $\Delta = 0{\cdot}009$, $N = 112$. The size of $\sigma$ is indicated by a heavy horizontal line running from $-\sigma$ to $\sigma$ at the top of the figure.

6]. An interesting implication is that one should be able to formulate a model in terms of interactions between clusters of clones.

For $\sigma = 0{\cdot}016$, we display in Fig. 6 two different equilibrium distributions. The only difference between Figs 5(a), 6(a) and (b) is the (random) initial condition. Varying only the random number seed used to generate the initial random distribution, we have simulated a total of ten of these networks. Each of these attained a different equilibrium distribution. The distribution of antibodies present in an animal is called its repertoire. We conclude that the immune repertoire of this shape-space model has a high degree of plasticity. The immunological implication of this is that external influences, such as self or foreign antigens, may easily influence the repertoire of the network. One common feature of all the repertoires that are attained is the large autobody located around the origin of the shape-space.

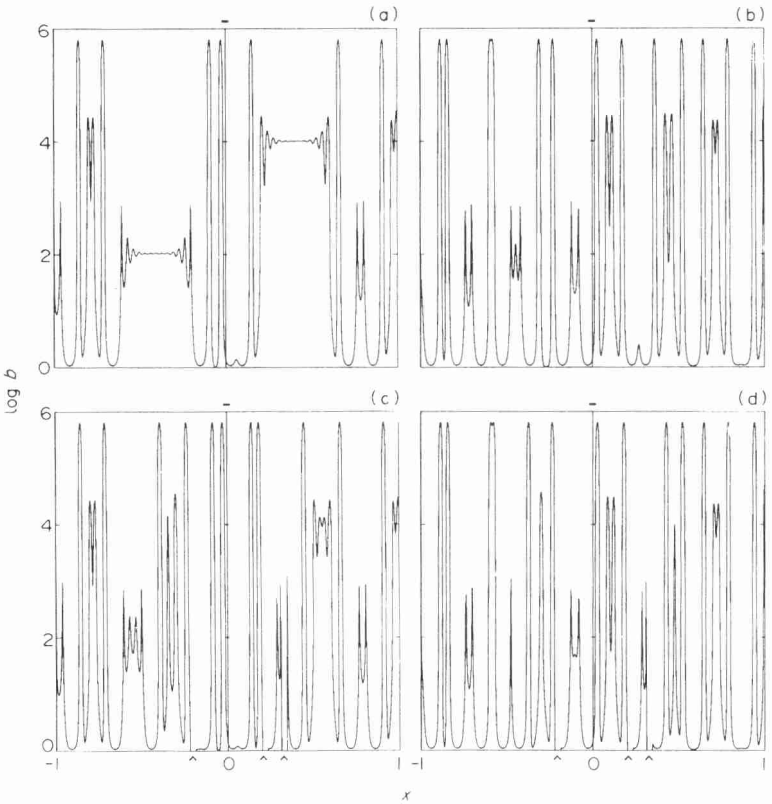


FIG. 6. Steady-state B cell population distributions for the model studied in Fig. 5(a). Parameters as in Fig. 5 except $\sigma = 0{\cdot}016$, $\Lambda = 0{\cdot}003$, $N = 316$. (a) and (b) differ from Fig. 5(a) only in the seed of the random number generator used to generate the initial population distribution. (c) and (d) show the same networks as (a) and (b) but with three self antigens located at $x = -0{\cdot}20$, $0{\cdot}21$, $0{\cdot}33$ (arrows).

### 3.5. SELF ANTIGENS

Coutinho (1989) and Holmberg *et al.* (1989) argue that the interaction between the environment of self-antigens and the developing immune network determines repertoire selection. Having found considerable plasticity in potential repertoires, we indeed expect that self-antigens will influence the selection of the actual repertoire. We now investigate this matter.

Within the shape-space framework, any particular antigen will also have a shape $x$, where $-L \leq x \leq L$, and its concentration $a(x)$ will influence the field of complementary B cell clones. Complete incorporation of antigen would modify eqn (3) into

$$h(x, b) = \int_{-L}^{L} g(x, \hat{x})[b(\hat{x}, t) + a(\hat{x}, t)]\, \mathrm{d}\hat{x}, \tag{27}$$

and would require an additional equation for $a$ specifying antigen dynamics. For self-antigens, which we expect to be present at constant concentration, so that $\partial a/\partial t = 0$, no new equation need be added. Further, self-antigens are thought to induce tolerance or non-responsiveness in clones that recognize them (cf. Goodnow *et al.*, 1988, 1990). To model this, for any self antigen of shape $x$ we eliminate clones of shapes in the range $(x-\sigma, x+\sigma)$. Clones within this region are deleted from the repertoire by omitting the source from the bone marrow (i.e. $m_x = 0$). Thus, tolerance induces holes of a width $2\sigma$ in the repertoire. In Fig. 6(c) and (d) we show the same networks with the same initial conditions as the ones shown in Fig. 6(a) and (b), respectively, but in the presence of three randomly chosen self antigens located at $x = -0{\cdot}20, 0{\cdot}21, 0{\cdot}33$. Because the repertoires in Fig. 6(a) and (b) differ from those in Fig. 6(c) and (d), we conclude that the self antigens do influence repertoire selection. Depending on how the deleted clones fit in the repertoire, this difference may either be substantial, as between Fig. 6(a) and (c), or may be minor, as betwen Fig. 6(b) and (d). Additionally, because the same three self-antigens select the different repertoires in Fig. 6(c)–(d), we conclude that even a self-referential repertoire may be sufficiently plastic to be able to reflect further environmental differences.

We have also studied the response to foreign antigens by implementing eqn (27). If an antigen is introduced in a stimulatory concentration, and contains sufficiently many epitopes (i.e. different shapes), it modifies the repertoire (not shown). Coutinho's and Holmberg's view is that immune responses to antigens do not come from the network but stem from the clonally organized compartment of the immune system. We show below that some idiotypes remain functionally disconnected from the network. Such shapes may therefore account for an immune response typical of a clonally organized immune system. Interestingly, whenever perturbations by antigens modify the repertoire, the disconnected shapes may become functionally connected to the network. This may account for a form of memory (Coutinho, 1989; De Boer & Perelson, 1991).

### 3.6. CLONAL ORGANIZATION

The question of whether or not the immune system combines a functional idiotypic network with a set of clones functionally disconnected from the network can be addressed by searching for regions in shape-space in which both the field and the B cell populations are small, indicating that B cells exist in the virgin state. Such cells would not be stimulated by the network and hence would be available to respond to antigen as perceived in the classical picture of clonal selection theory.

Virgin regions exist in the repertoires shown in Figs 2–6. They tend to be located adjacent to the high peaks (of order $\theta_3$) in the repertoire. The mere existence of these "virgin" regions fails to provide a conclusive answer to our question about the organization of the immune system, because the virgin regions occupy only a small proportion of the shape-space. We believe this may be an artifact due to the low dimensionality of the shape-space. Below, this question is addressed further with a 2-D shape-space model.

## 4. 2-D Shape-space—A Lattice Model

### 4.1. FURTHER SIMPLIFICATION

As a first step toward examining higher dimensional shape spaces, we shall consider a 2-D shape-space. The calculations required are considerably more time consuming than for the 1-D case, so that it is expedient to simplify our model. To this end we simplify eqn (1) by setting $m=0$. (Previously we assumed that $m \ll \theta_1$.) Thus, B cell dynamics are now regarded as governed by

$$\frac{1}{b}\frac{\partial b}{\partial t} = pf[h(x; b)] - 1. \tag{28a}$$

Changing variables to $B = \ln b$, we obtain

$$\frac{\partial B}{\partial t} = pf[h(x; B)] - 1, \tag{28b}$$

where for each shape $x$

$$h(x; B) = \int_{-L}^{L} g(x, \hat{x})\, e^{B(\hat{x},t)}\, d\hat{x}.$$

Changing to logarithmic variables has the advantage that the variation in the rate of increase of each population now cannot be large, for

$$-1 \leq \frac{\partial B}{\partial t} \leq p - 1 \approx 1.$$

Since (28b) is much less stiff than (28a), we can simplify eqn (28b) into the mapping

$$B(x, t+1) = B(x, t) + pf[h(x; B)] - 1, \tag{28c}$$

which is equivalent to using an Euler integration method with step size one.

We now generalize our considerations to a 2-D lattice mapping with shape variables $x$ and $y$ that are integers, $-N \leq x, y \leq N$. We propose a circular shape-space, i.e. one that is bounded by $x^2 + y^2 \leq N^2$. (The rationale for this is that shapes with extreme values of both $x$ and $y$ should be rare.) The field is now given by

$$h(x, y; B) = \Delta^2 \sum_{i,j \in C(-x,-y)} g(x, y, i, j)\, e^{B(i,j,t)}, \qquad x^2 + y^2 \leq N^2. \tag{29}$$

In (29), $C(-x, -y) \equiv \{i, j \mid (i+x)^2 + (j+y)^2 \leq n^2, i^2 + j^2 \leq N^2\}$ is the portion of the circle centered at $(-x, -y)$ with radius $n$ that lies within the circular shape space of radius $N$. The function $g(x, y, i, j)$ is the two-dimensional Gaussian

$$g(x, y, i, j) = (2\pi\sigma^2)^{-1} \exp\{-\Delta^2[(x+i)^2 + (y+j)^2]/2\sigma^2\}. \tag{30}$$

Note that (29) incorporates fixed boundary conditions: the clones outside $x^2 + y^2 = N^2$ make no contribution to any of the fields.

To complete our model at this stage, the mapping (28c) is made two-dimensional. Moreover, we require that populations $B(x, y)$ never become smaller than zero (note that $B=0$ corresponds to $b=1$, i.e. to one B cell). This yields

$$B(x, y, t+1)=\max\,[0,\, B(x, y, t)+pf\,[h(x, y; B)]-1], \qquad x^2+y^2\leq N^2. \quad (31)$$

### 4.3. THE 2-D LATTICE MAPPING

The standard way of formulating a discrete time lattice model is to develop transition rules that depend on some finite (and usually local) neighborhood of each cell in the lattice. The fact that we do not consider a standard local neighborhood, but instead the neighborhood around the cell having complementary co-ordinates, introduces non-locality in the lattice. Hence, processes in one region in the lattice influence processes in other distant regions.

Since the model of (29–31) is defined in terms of an infinite Gaussian function, we introduce a cut-off point below which interactions are assumed negligible. To implement the cut-off, we truncate the 2-D Gaussian so that terms with amplitude below $10^{-3}$ are set to zero. This implies that the field is non-zero only over a neighborhood of a certain radius. By eqn (30) this radius depends on the parameters $\sigma$ and $\Delta$.

The introduction of an affinity cut-off seems realistic because interactions at affinities below $10^4$ M$^{-1}$ or $5\times10^4$ M$^{-1}$ do not seem to lead to B cell stimulation (Fish *et al.*, 1989; Riley & Klinman, 1986; Klinman, 1972). Additionally, we have seen in eqns (25e–26a) that the minimal affinity $\varepsilon$ limits the maximal size that each individual population can attain. Thus an affinity cut-off of $\varepsilon=10^{-3}$, defining the smallest possible self-stimulation, sets the maximum self-stimulatory population to roughly $\theta_2/\varepsilon=10^7$. Since the maximum population size and the minimum affinity are coupled this way, we seem to have two choices for preventing populations growing extremely large. The most natural choice in the lattice mapping seems to be a finite neighborhood. The most natural choice in the discrete approximation to the continuous PDE model seems to be the maximum population size. See Appendix for some technical subtleties that arise because we have set $m=0$.

We have studied the lattice mapping for $N=50$, $\Delta=0{\cdot}02$, $(L=1)$, $p=2$, $\theta_1=10^2$, $\theta_2=10^4$, and several values of $\sigma$. Figures 7–9 display the distribution of clone and field sizes that were attained after 500 time steps for $\sigma=0{\cdot}022$, $0{\cdot}031$, $0{\cdot}063$. The radius of the circular neighborhood was $n=4$, 5, 8 in these three cases, respectively. At $t=0$ each square in the lattice was assigned a random value distributed around the maximum of the bell shaped function, i.e. $B=\ln\sqrt{\theta_1\theta_2}$, with 10% standard deviation. At each location $(x, y)$ the gray scale indicates the size of the clone $B(x, y)$ (left panels) and the size of the field $\ln h(x, y)$ (right panels). The gray scales displayed in Figs 7–9 display roughly circular patterns. The patterns are reminiscent of those typically found in reaction–diffusion systems. Were we to use the standard square local neighborhood, instead of the circular Gaussian neighborhood used here, the patterns would be more rectangular.

The pattern formation depends on the non-locality that is introduced by the complementary neighborhoods. If we change the neighborhood relation into the standard

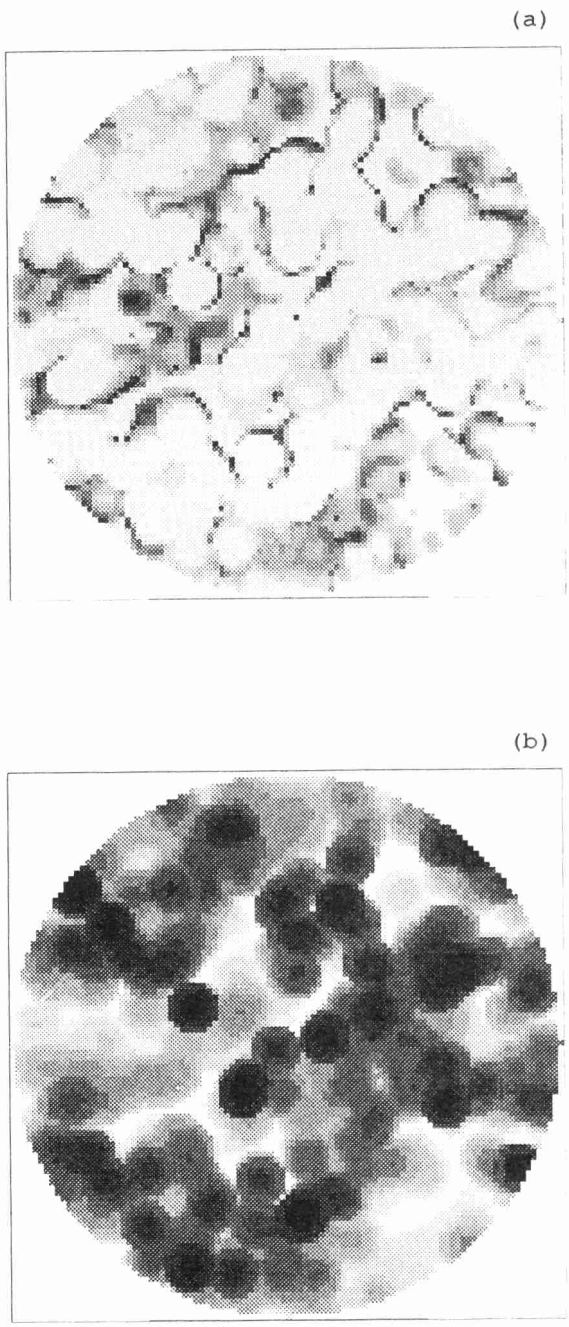


FIG. 7. 2-D patterns in the lattice mapping, eqn (31), after 500 iterations. Parameters: $p=2$, $\theta_1=10^2$, $\theta_2=10^4$, $L=1$, $N=50$, $\Delta=0{\cdot}02$, $\sigma=0{\cdot}022$. (a) Population sizes: black corresponds to $B=20$, light gray corresponds to $B=0$. (b) Field sizes: black corresponds to $\ln h=17$, white corresponds to $\ln h=0$.

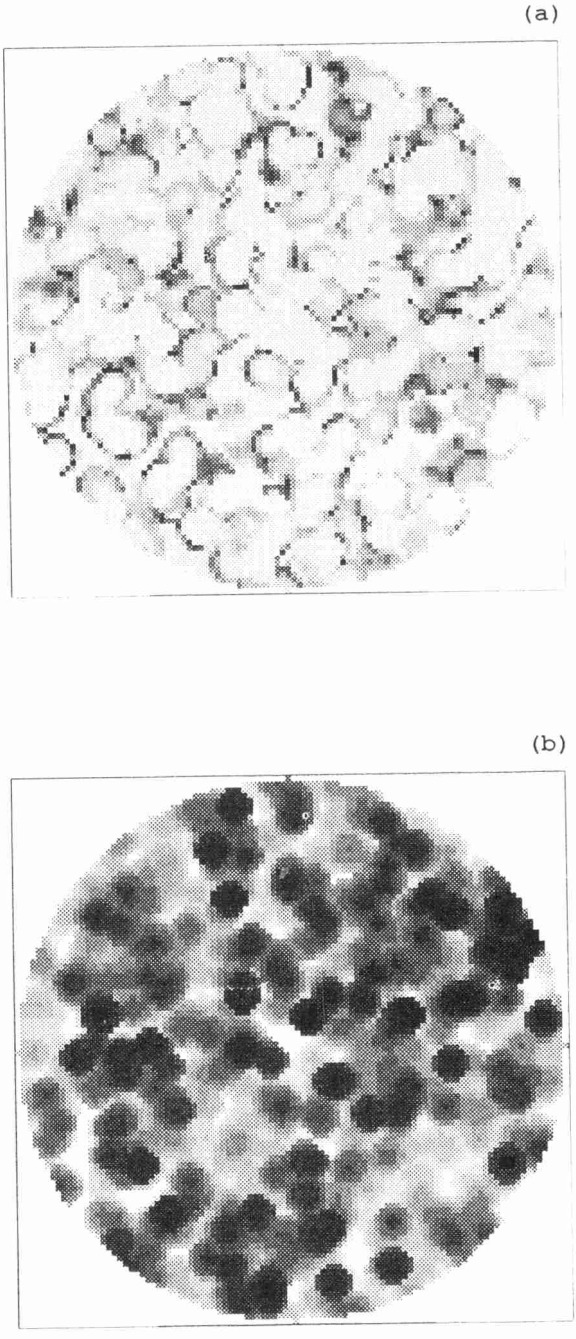


FIG. 8. As Fig. 7, but $\sigma = 0{\cdot}032$. (a) Population sizes. (b) Field sizes (here black corresponds to $\ln h = 16$).

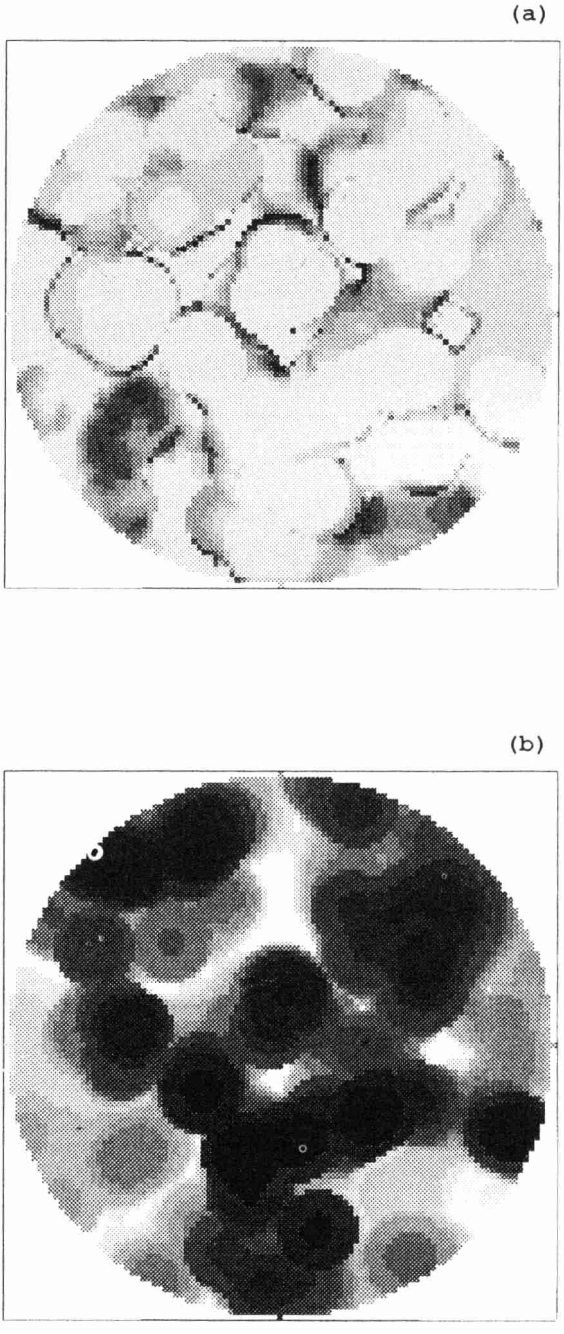


FIG. 9. As Fig. 7, but $\sigma = 0{\cdot}063$. (a) Population sizes. (b) Field sizes (here black corresponds to $\ln h = 15$).

local neighborhood, we find no pattern at all. Conversely, if we assume complementarity in one direction, but a local neighborhood in the other direction, we find patterns that are very similar to the patterns shown in Figs 7–9. Different matching rules in different directions allow different properties of the binding site to be expressed. The interpretation of complementarity could for instance be a geometrical fit; the interpretation of a local neighborhood could for instance be hydrophobicity. Other properties, such as charge, require other (non-local) neighbor relations.

The distributions of clone sizes and field values in Figs 7–9 form landscapes of roughly circular hills and valleys. These patterns resemble the distributions of the 1-D shape-space shown in Figs 2–6 in a number of ways. First, the field patterns are wider and rounder than that of the clone patterns. Second, the ridges and hills in the 2-D clone patterns correspond to the peaks and clusters in the 1-D clone patterns. Superimposing the clone and the field distributions reveals that the large clones are typically located at intermediate field values, i.e. at values between $\theta_1$ and $\theta_2$. Thus, the dark ridges of large clones correspond to contour lines of intermediate height in the field landscape. Third, as the variance of the Gaussian is made smaller, more peaks and valleys appear. Thus, the scale of the pattern increases with $\sigma$.

The $t = 500$ distributions displayed in Figs 7–9 are not in a steady state. To illustrate this, we show in Fig. 10(a)–(d), how clone sizes at four points in the shape-space vary with time. As can be seen, the clone sizes fluctuate over several orders of magnitude, in 2–4 weeks. Some points may remain empty [i.e. $B(x, y) = 0$] over comparable periods of time, as illustrated in Fig. 10. The oscillatory behavior does not seem to depend on the variance $\sigma^2$. Inspection of the global pattern as it evolves in time reveals that the landscape of hills and valleys changes slowly (not shown), typically over several months. Thus, although clone sizes change on a rapid time scale, the global pattern seems to be more conserved and changes on a slower time scale. The same is true in the 1-D shape-space. We have described above how the clusters may oscillate for a long time without changing their location in space.

### 4.4. CLONAL ORGANIZATION

In the 1-D shape-space and in the 2-D lattice mapping we have scored the number of shapes that have a field and a clone size that are smaller than $\theta_1/10$. We call these the *disconnected* clones. Such shapes are only poorly stimulated by the network, and correspond to clones that would behave according to the tenets of classical antigen-driven clonal selection theory (Burnet, 1959). As a function of $\sigma$, we plot in Fig. 11 the average percentage of disconnected clones in 1-D (○) and in 2-D (●) shape-spaces. For both the 1-D and the 2-D shape-space, *increasing $\sigma$ increases the percentage of disconnected clones*. This may seem counterintuitive because an increase in $\sigma$, i.e. the cross-reactivity of each clone, should increase the connectedness of the network. The explanation seems to be that increasing $\sigma$ causes the scale of the patterns to increase. This creates large valleys where both clones and fields are small.

Even more striking is the difference between the 1-D and the 2-D shape-space. Apparently, increasing the dimension of the space increases the scale of the patterns, and hence the percentage of disconnected clones. An extrapolation from Fig. 11 into

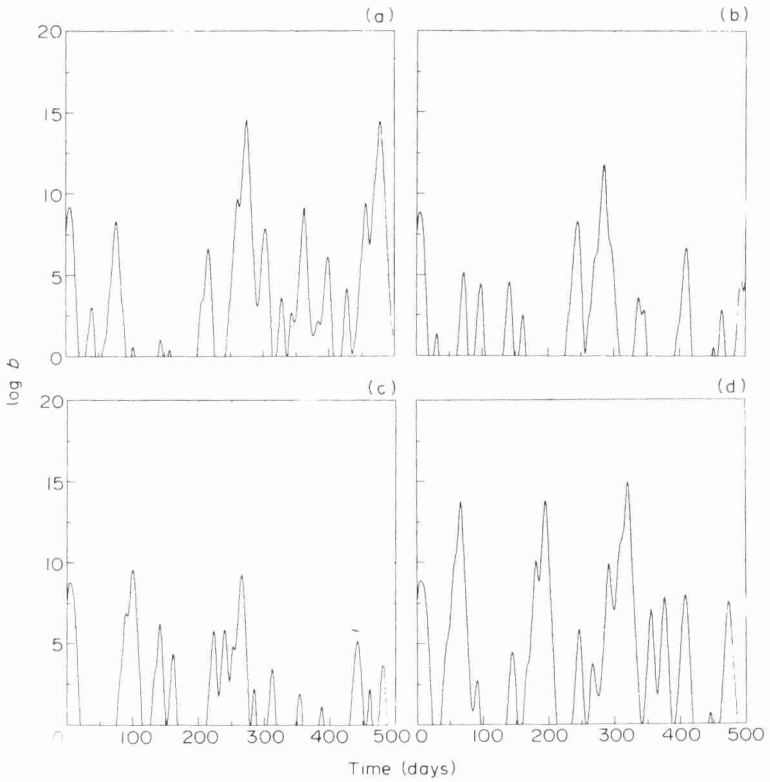


FIG. 10. Dynamic changes in the population size of the clone located at $(N/2, N/2)$ in the lattice mapping of Fig. 7 for various values of $\sigma$. (a) $\sigma = 0{\cdot}016$. (b) $\sigma = 0{\cdot}032$. (c) $\sigma = 0{\cdot}045$. (d) $\sigma = 0{\cdot}063$.

a higher dimensional shape-space would predict that it should be possible to obtain a substantial percentage of disconnected clones. Whether this percentage can approach the 80–90% of disconnected clones that Coutinho (1989) and Holmberg *et al.* (1989) estimate remains unknown.

The effect of an increase in dimensionality is two-fold. First, for equal values of $\sigma$, a 2-D shape-space has a higher percentage of disconnected clones. Second, comparing Fig. 5(c) with Fig. 8, for both of which $\sigma = 0{\cdot}032$ we see that, the 2-D shape-space seems to allow for more local peaks. Thus, if the number of local peaks were to correspond to the number of specificities in the repertoire, it would seem that the 2-D shape-space allows for a higher value of $\sigma$. Figure 11 suggests that this would increase the percentage of disconnected clones.

## 5. Discussion

We have modified an earlier shape-space model (Segel & Perelson, 1988) so as to take into account the bell-shaped B cell activation function that has characterized

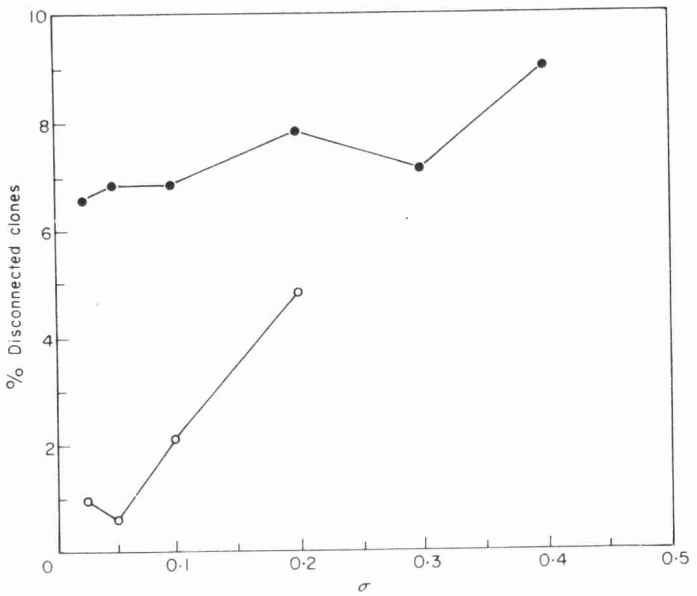


FIG. 11. The average percentage of disconnected clones at $t = 500$ in 1-D (○) and 2-D (●) shape-spaces. Each (●) is the average of four 2-D simulations, each (○) is the average of five 1-D simulations.

much recent network modeling (cf. De Boer, 1988; De Boer & Hogeweg, 1989*a–c*; De Boer *et al.*, 1990; De Boer & Perelson, 1991; Weisbuch *et al.*, 1990; Perelson & Weisbuch, 1992). Whereas the original Segel–Perelson model had only one uniform steady state, the virgin state, this model has three: virgin, immune and suppressed. We have argued previously (Segel & Perelson, 1988) that one important characteristic of the virgin state is that it be stable but not too stable. Stability is important so that small random perturbations do not excite the system. However, the virgin state should not be so stable that a large perturbation, say by antigen, leads to no appreciable response. For the current model, we have shown that the virgin state is stable to both uniform and sinusoidal perturbations. To keep this state from being too stable requires setting the parameters of the system near the stability boundary. This can easily be done by adjusting $\theta_1$, the threshold for activation in the bell-shaped function.

In addition to the virgin state, our model has immune and suppressed states that are sustained by network activity. We showed that homogeneous immune and suppressed states are unstable to sinusoidal perturbation. Thus, the entire immune system cannot remain in a homogeneous activated state. Perturbing the system from either the homogeneous, immune, or suppressed state leads to the formation of a pattern of activity in shape-space, with, roughly speaking, some clones immune, some suppressed, and others virgin. The generation of pattern in this system does not rely upon short-range activation and long-range inhibition.

Segel & Perelson (1988) considered a model that was similar in many respects to the model considered here. Their basic equation was similar to (1), but included two exponentials limiting the total number of B cells and the maximum clone size, respectively. Their definition of the field [corresponding to eqns (3) and (4)] was the same as those used here. Instead of employing the biphasic function (2), Segel & Perelson (1988) treated activation $a$ and suppression $s$ separately. Different standard deviations $\sigma_a$ and $\sigma_s$ were used in calculating the fields $h_a$ and $h_s$ for activation and suppression, respectively. Segel and Perelson were seeking a reaction–diffusion type instability of the uniform state. Hence, they assumed a long range inhibition and a short range activation ($\sigma_s > \sigma_a$), although later they showed that this assumption could be reversed and the effect would be the same (Segel & Perelson, 1990). It should be borne in mind, however, that the requirement of relatively long-range inhibition in reaction–diffusion theory is a consequence of the effort to bring about instability to small perturbations at a "most dangerous" wavelength that is positive. In particular "most dangerous" perturbations of infinite or zero wavelengths are usually regarded as unacceptable in reaction–diffusion theory. The reason is that if linear theory predicts instability at an intermediate wavelength then one has a good idea of the pattern wavelength that in fact emerges from the non-linear equations—without resorting to extremely demanding non-linear calculations. Thus, one can without difficulty compare one's predictions with observed patterns.

The situation is different in the present instance. Here a primary goal is not to predict observed instability patterns but rather is to arrange conditions so that the virgin state is stable but not too stable. Hence, it is quite admissible to consider instabilities at zero or infinite wavelength in seeking the stability boundary. There is therefore no reason to restrict oneself to relatively long range inhibition, and indeed our model contains only a single "range". Note that there is still a pattern that develops from the infinite wavelength instability of the suppressed state, a pattern that is strongly influenced by non-linear effects.

In previous models in which antibodies or B cells were characterized as being in levels, $Ab_1, Ab_2, \ldots$, where antibodies on level 1 are complementary to those on level 2, etc, we found that immune and suppressed states tend to alternate. For example, $Ab_1$ immune, $Ab_2$ suppressed, $Ab_i$ virgin, $i = 3, 4, \ldots$ was a possible (localized) steady state (Weisbuch *et al.*, 1990). Depending on network topology and parameter values, "percolating" states could also occur in which the entire immune system is activated; e.g. $Ab_1$ immune, $Ab_2$ suppressed, $Ab_3$ immune, $Ab_4$ suppressed, etc. (De Boer & Hogeweg, 1989*b*). The characteristic of all these possible steady states is that clones in the immune state that have high population tend to suppress clones connected to them, but the suppressed clones settle at population levels sufficiently higher than virgin that they can sustain the activation of the immune clone. In our current model there is no *a priori* assignment of clones to levels, yet we still see that in patterns that form spontaneously clusters of immune clones will lie in regions of shape-space that are complementary to clusters of suppressed clones. This is not surprising since the bell-shaped activation function requires an immune clone to see a low field as generated by a suppressed population, and a suppressed clone to see a high field of the type generated by an immune clone. What is surprising

is that we find localized regions of shape-space, of width much larger than the field sensed by any single clone, in which all clones are activated. Further, this region is complementary in shape to a region of roughly equal width in which all clones are suppressed [Fig. 6(a)]. These higher order localized structures seem to be emergent properties of our model.

Another interesting feature of the patterns developed by the model is that for small values of $\sigma$ there is not one stable pattern but many possible ones. The pattern of clone sizes reflects the antibody repertoire of an animal. Thus, our model is consistent with many possible repertoires, the one actually present in an animal being dependent of the presence of self-antigen, encounters with foreign antigen and any other feature that can affect the initial conditions applied in the model. These observations are consistent with each animal having a unique potential immune system reactivity that is dependent upon its history of antigenic exposure.

To further characterize patterns in shape-space we developed a 2-D lattice mapping. The results obtained with these 2-D shape-spaces bear resemblance to recent results obtained by Stewart & Varela (1991) with a different 2-D shape-space model. Technically the two models differ significantly. First, Stewart & Varela consider only two complementary idiotype species, black and white, that interact whenever their distance in shape-space is sufficiently small. Second, their model neglects population dynamics. That is, rather than dealing with gray scales that indicate population sizes, they regard clones as either present or absent. Clones are present if they receive a degree of stimulation that falls between two thresholds (that are comparable to our $\theta_1$ and $\theta_2$). Patterns evolve by the introduction of novel shapes from the bone marrow. Novel shapes are only incorporated if their field falls within the stimulation window. If they are incorporated they change the fields of nearby clones. This, in turn, can lead to the elimination of those clones having a field outside the window. The pattern is updated until a coherent field is found. In contrast, since our shape-space incorporates all possible shapes, we assume that new cells emerging from the bone marrow are not unique, and thus may be merged with one of the pre-existing populations. Thus, in our model pattern changes are driven by changes in population size, and not by the introduction of novel clones *per se*.

In our simplest model of idiotypic B cell proliferation cell populations grow extremely large to compensate for low-affinity interactions. Since interaction terms are typically of the form *affinity* × *concentration*, the effect may be realistic. Two properties of the model that are responsible for the extremely large populations are unrealistic however. First, as we have argued above, we need an affinity cut-off to account for the fact that low affinity antibodies are unable to stimulate B cells, even at high concentrations. However, because affinities of IgG antibodies may vary over six orders of magnitude, our model would still allow populations to grow by six orders of magnitude. This remains unrealistic. Antibodies of type IgM, which tend to be found in early networks, typically are all of low affinity, e.g. $10^4$–$10^5$ M$^{-1}$ and thus this discrepancy in population levels may not appear for IgM interactions. Second, and more important, these artificially high population levels are probably due to the fact that in our model stimulated B cells fail to stop proliferating, although experiments suggest that B cells at a maximum go through eight rounds of cell division

(cf. Klinman *et al.*, 1974). Usually, activated B cells mature into plasma cells, which produce antibody but do not divide. If our model were to incorporate B cell maturation into a non-dividing end-stage cell, as has been done in earlier models (Bell, 1970, 1971; Perelson *et al.*, 1976, 1978), we would achieve a model in which the individual populations remain bounded without the aid of the population limitation that we have introduced here. The relative roles of various means for population limitation remain to be assessed.

Whether or not the immune network is able to combine a fully connected network with a clonal organization of part of the repertoire is partly answered by the current shape-space analysis. We do find regions of the shape-space where the field is so low that clones remain virgin. Clones in these regions are capable of responding to foreign antigens according to the tenets of classical clonal selection theory. The low ratios between virgin and stimulated clones that we find seem to be at variance with the ratios reported in the empirical literature, i.e. 10–20% in the network and 80–90% disconnected clones. However, the results suggest that shape-spaces of higher dimension might support large scale patterns that contain a higher percentage of disconnected clones. This is to be addressed in future research.

The work described here was performed under the auspices of the U.S. Department of Energy, and supported in part by NIH Grants AI 28433 and RR06555, the U.S.-Israel Binational Science Foundation Grant 89-00146, and by the Santa Fe Institute through their Theoretical Immunology Program. We thank Dr John Stewart for discussing his work with Varela on their 2-D shape-space formalism, and making their unpublished manuscipt available to us.

## REFERENCES

Amit, A. G., Mariuzza, R. A., Phillips, S. E. V. & Poljak, R. J. (1986). Three-dimensional structure of an antigen–antibody complex at 2.8 Å resolution. *Science* **233,** 747–753.

Bell, G. (1970). Mathematical model of clonal selection and antibody production. *J. theor. Biol.* **29,** 191–232.

Bell, G. (1971). Mathematical model of clonal selection and antibody production. II. *J. theor. Biol.* **33,** 339–378.

Burnet, F. M. (1959). *The Clonal Selection Theory of Acquired Immunity*. London: Cambridge University Press.

Coutinho, A. (1989). Beyond clonal selection and network. *Immunol. Revs.* **110,** 63–87.

De Boer, R. J. (1988). Symmetric idiotypic networks: connectance and switching, stability, and suppression. In: *Theoretical Immunology Part Two* (Perelson, A. S., ed.) pp. 265–289. *SFI Studies in the Science of Complexity* Vol. III. Redwood City, CA: Addison-Wesley.

De Boer, R. J. & Hogeweg, P. (1989*a*). Memory but no suppression in low-dimensional symmetric idiotypic networks. *Bull. math. Biol.* **51,** 223–246.

De Boer, R. J. & Hogeweg, P. (1989*b*). Unreasonable implications of reasonable idiotypic network assumptions. *Bull. math. Biol.* **51,** 381–408.

De Boer, R. J. & Hogeweg, P. (1989*c*). Idiotypic network models incorporating T–B cell co-operation: the conditions for percolation. *J. theor. Biol.* **139,** 17–38.

De Boer, R. J., Kevrekidis, I. G. & Perelson, A. S. (1990). A simple idiotypic network model with complex dynamics. *Chem. Engng. Sci.* **45,** 2375–2382.

De Boer, R. J. & Perelson, A. S. (1991). Size and connectivity as emergent properties of a developing immune network. *J. theor. Biol.* **149,** 381–424.

Dembo, M. & Goldstein, B. (1978). Theory of equilibrium binding of symmetric bivalent haptens to cell surface antibody: application to histamine release from basophils. *J. Immunol.* **121,** 345–353.

FARMER, J. D., PACKARD, N. H. & PERELSON, A. S. (1986). The immune system, adaptation and machine learning, *Physica* **22D**, 187–204.

FISH, S., ZENOWICH, E., FLEMING, M. & MANSER, T. (1989). Molecular analysis of original antigenic sin. I. Clonal selection, somatic mutation, and isotype switching during a memory B cell response. *J. exp. Med.* **170,** 1191–1209.

GOODNOW, C. C., ADELSTEIN, S. & BASTEN, A. (1990). The need for central and peripheral tolerance in the B cell repertoire. *Science* **248,** 1373–1379.

GOODNOW, C. C., CROSBIE, J., ADELSTEIN, S., LAVOIE, T. B., SMITH-GILL, S. J., BRINK, R. A., PRITCHARD-BRISCOE, H., WOTHERSPON, J. S., LOBLAY, R. H., RAPHAEL, K., TRENT, R. J. & BASTEN, A. (1988). Altered immunoglobulin expression and functional silencing of self-reactive B lymphocytes in transgenic mice. *Nature, Lond.* **334,** 676–682.

HOLMBERG, D., ANDERSSON, Å., CARLSON, L. & FORSGEN, S. (1989). Establishment and functional implications of B-cell connectivity. *Immunol. Rev.* **110,** 89–103.

JERNE, N. K. (1974). Towards a network theory of the immune system. *Ann. Immunol. (Inst. Pasteur)* **125C,** 373–389.

KANG, C.-Y. & KÖHLER, H. (1986*a*). Immunoglobulin with complementary paratope and idiotope. *J. exp. Med.* **163,** 787–796.

KANG, C.-Y. & KÖHLER, H. (1986*b*). A novel chimeric antibody with circular network characteristics: autobody. *Ann. N.Y. Acad. Sci.* **475,** 114–122.

KLINMAN, N. R. (1972). The mechanism of antigenic stimulation of primary and secondary clonal precursor cells. *J. exp. Med.* **136,** 241–260.

KLINMAN, N. R., PRESS, J. L., PICKARD, A. R., WOODLAND, R. T. & DEWEY, A. F. (1974). Biography of the B cell. In: *The Immune System, Genes, Receptors, Signals* (Sercarz, E. E., Williamson, A. R. & Fox, C. F., eds) pp. 357–365. New York: Academic Press.

PERCUS, J. (1988). Polydisperity in immune networks. In: *Theoretical Immunology, Part Two* (Perelson, A. S., ed.) pp. 345–358. *SFI Studies in the Science of Complexity* Vol. III. Redwood City, CA: Addison-Wesley.

PERCUS, J. (1989). Tree structures in immunology. In: *Applications of Combinatorics and Graph Theory to the Biological and Social Sciences* (Roberts, F., ed.) pp. 259–276. New York: Springer-Verlag.

PERELSON, A. S. (1984). Some mathematical models of receptor clustering by multivalent ligands. In: *Cell Surface Dynamics: Concepts and Models* (Perelson, A. S., DeLisi, C. & Wiegel, F. M., eds) pp. 223–276. New York: Marcel Dekker.

PERELSON, A. S. & DELISI, C. (1980). Receptor clustering on a cell surface. I. Theory of receptor cross-linking by ligands bearing two chemically identical functional groups. *Math. Biosci.* **48,** 71–110.

PERELSON, A. S., MIRMIRANI, M. & OSTER, G. F. (1976). Optimal strategies in immunology, I. B-cell differentiation and proliferation. *J. math. Biol.* **3,** 325–367.

PERELSON, A. S., MIRMIRANI, M. & OSTER, G. F. (1978). Optimal strategies in immunology, II. B memory cell production. *J. math. Biol.* **5,** 213–256.

PERELSON, A. S. & OSTER, G. F. (1979). Theoretical studies on clonal selection: minimal antibody repertoire size and reliability of self–non-self discrimination. *J. theor. Biol.* **81,** 645–670.

PERELSON, A. S. & WEISBUCH, G. (1992). Modeling immune reactivity in secondary lymphoid organs. *Bull. Math. Biol.* **53,** in press.

PRESS, W. H., FLANNERY, B. P., TEUKOLSKY, S. A. & VETTERLING, W. T. (1988). *Numerical Recipes in C. The Art of Scientific Computing.* Cambridge: Cambridge University Press.

RILEY, R. L. & KLINMAN, N. R. (1986). The affinity threshold for antigenic triggering differs for tolerance susceptible immature precursors vs. mature primary B cells. *J. Immunol.* **136,** 3147–3154.

SEGEL, L. A. & PERELSON, A. S. (1988). Computations in shape-space: a new approach to immune network theory. In: *Theoretical Immunology, Part Two* (Perelson, A. S., ed.) pp. 321–343. *SFI Studies in the Science of Complexity* Vol. III. Redwood City, CA: Addison-Wesley.

SEGEL, L. A. & PERELSON, A. S. (1989). Shape-space analysis of immune networks. In: *Cell to Cell Signalling: From Experiments to Theoretical Models* (Goldbeter, A., ed.) pp. 273–283. New York: Academic Press.

SEGEL, L. A. & PERELSON, A. S. (1990). A paradoxical instability caused by relatively short range inhibition. *Siam J. appl. Math.* **50,** 91–107.

SEGEL, L. A. & PERELSON, A. S. (1991). On the shape-space approach to the immune system: A B cell antibody model. *J. Stat. Phys.* **63,** 1113–1131.

SHERIFF, S., SILVERTON, E. W., PADLAN, E. A., COHEN, G. H., SMITH-GILL, S. J. FINZEL, B. C. & DAVIES, D. R. (1987). Three-dimensional structure of an antibody-antigen complex. *Science* **84,** 8075–8079.

STANFIELD, R. L., FIESER, T. M., LERNER, R. A. & WILSON, I. A. (1990). Crystal structures of an antibody to a peptide and its complex with peptide and its complex with peptide antigen at 2.8 Å. *Science* **248,** 712–719.

STEWART, J. & VARELA, F. J. (1990). Dynamics of a class of immune networks. II. Oscillatory activity of cellular and humoral components. *J. theor. Biol.* **144,** 103–115.

STEWART, J. & VARELA, F. J. (1991). Morphogenesis in shape-space. Elementary meta-dynamics in a model of the immune network. *J. theor. Biol.* **153,** 477–498.

VARELA, F. J., COUTINHO, A., DUPIRE, B. & VAZ, N. N. (1988). Cognitive networks: immune, neural, and otherwise. In: *Theoretical Immunology, Part Two* (Perelson, A. S., ed.) pp. 359–375. *SFI Studies in the Science of Complexity* Vol. III. Redwood City, CA: Addison-Wesley.

WEINAND, R. G. (1990). Somatic mutation, affinity maturation and the antibody repertoire: a computer model. *J. theor. Biol.* **143,** 343–382.

WEINAND, R. G. (1991). Somatic mutation and the antibody repertoire: a computational model of shape-space. In: *Molecular Evolution on Rugged Landscapes* (Perelson, A. S. & Kauffman, S. A., eds) pp. 215–236. *SFI Studies in the Science of Complexity* Vol. IX. Redwood City, CA: Addison-Wesley.

WEISBUCH, G. (1990). A shape-space approach to the dynamics of the immune system. *J. theor. Biol.* **143,** 507–522.

WEISBUCH, G., DE BOER, R. J. & PERELSON, A. S. (1990). Localized memories in idiotypic networks. *J. theor. Biol.* **146,** 483–499.

## APPENDIX

To transform our differential equation model into a mapping we omitted the source of cells from the bone marrow, i.e. we set $m=0$. Since the source was small in any case, i.e. $m \ll \theta_1$, this seems to be a reasonable assumption. However, stimulating the differential equation model eqn (25) for $m_i=0$, gave us very different results from those shown in Fig. 5 for $m_i=1$. Instead of having peaks centered around maxima of either $\theta_1$, $\theta_2$, or $\theta_3$, all peaks had a maximum of about $\theta_3$. Simulating a 2-D lattice mapping in which we incorporated a maximum population size of $\ln \theta_3$, the only peaks that were attained were comprised of clones at $\ln \theta_3$.

We give two indications that setting $m_i=0$ reduces the plasticity of the system because it eliminates steady-state solutions. First, the virgin state normally as $\bar{b}=m$, collapses to the origin. This leads to the elimination of all virgin clones as well as solutions that depend on virgin clones to maintain other clones in a non-virgin state. As an example, consider the possible steady states of the two species system

$$\frac{db_1}{dt} = m + b_1[pf(J_{11}b_1 + J_{12}b_2) - 1] = 0, \tag{A.1}$$

$$\frac{db_2}{dt} = m + b_2[pf(J_{12}b_1 + J_{22}b_2) - 1] = 0, \tag{A.2}$$

where we have set $J_{21}=J_{12}$. To determine the steady state, we substitute eqn (2) for $f(h)$ into eqn (A.1) and solve the resulting quadratic equation for $b_2$. Substituting into eqn (A.2), rearranging and squaring to remove radicals, we obtain a 12th-order polynomial equation for the steady-state value of $b_1$. Setting $m=0$ converts this polynomial into $b_1^6$ times a sixth-order polynomial. Thus six solutions collapse into the trivial solution $b_1=0$ when $m=0$. This shows that one loses non-trivial solutions by eliminating the source.

Second, we numerically studied a similar system with three populations where the second species was connected to species one and three. The interaction matrix, **J**, was given by

$$\mathbf{J}=\begin{pmatrix} 0 & 0{\cdot}5 & 0 \\ 0{\cdot}5 & 0 & 1 \\ 0 & 1 & 0 \end{pmatrix}.$$

Here the coupling between $b_2$ and $b_3$ is twice that of $b_2$ with $b_1$. In the presence of a source term one of the equilibria of this system is an immune state of $b_2$ that is maintained by both $b_1$ and $b_3$. For $m=10$, we find $b_2 \approx 2\theta_2$, $b_1 \approx 2\theta_1$, and $b_3 \approx 0{\cdot}5\theta_1$ [Fig. A1(a)]. In order to suppress $b_1$, $b_2$ needs to be of order $2\theta_2$, since at a suppressive steady state with $p=2$

$$f(h_1)=\frac{\theta_2}{\theta_2+0{\cdot}5b_2}=\frac{1}{p}=\frac{1}{2}.$$

Since $b_2=2\theta_2$ doubles the suppression on $b_3$, $b_3$ attains a population size that is intermediate between the suppressed and the virgin state. Such an intermediate state can only exist if $m>0$. This is illustrated in Fig. A1(a), which shows the equilibrium population levels of the three populations as a function of $m$. Decreasing $m$ decreases $b_3$ until it disappears. Note that it is $b_3$ that is excluded, i.e. it is again the lowest affinity interaction that dominates.

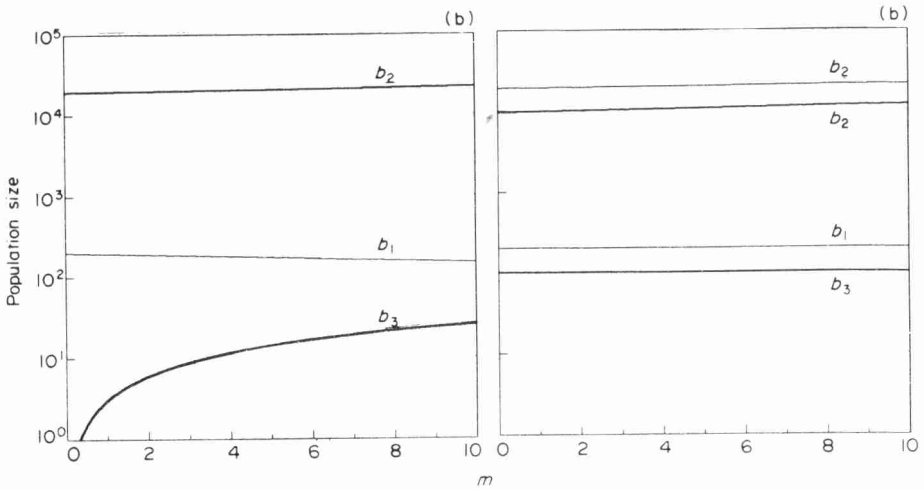


FIG. A1. The equilibrium populations in a 3-D or 2-D network as a function of the source $m$. Parameters: $p=2$, $\theta_1=10^3$, $\theta_2=10^4$. (a) In a 3-D network the clone with the highest affinity disappears when $m=0$. (b) In a 2-D subnetwork with a high affinity, i.e. $J_{12}=J_{21}=0$, $J_{23}=J_{32}=1$ (heavy lines), or a low affinity interaction, i.e. $J_{12}=J_{21}=0{\cdot}5$, $J_{23}=J_{32}=0$ (light lines), the B cell population sizes are hardly dependent on $m$.

For comparison, we show in Fig. A1(b) the same immune state in the absence of $b_3$, for $J_{12}=J_{21}=0{\cdot}5$ (the light lines), and in the absence of $b_1$, for $J_{23}=J_{32}=1$ (the heavy lines).

These findings suggest that eliminating the source term may significantly reduce the number of equilibria. In particular the coexistence of several clones of different affinity around either the immune or the suppressed state may become unlikely.